Mon. Not. R. Astron. Soc. **000**, 000–000 (0000) Printed 25 July 2014 (MN LATEX style file v2.2)

Numerical simulations of a shock interacting with multiple magnetized clouds

R. Alūzas[1⋆], J. M. Pittard[1], S. A. E. G. Falle[2], T. W. Hartquist[1]
[1] *School of Physics and Astronomy, University of Leeds, Woodhouse Lane, Leeds LS2 9JT, UK*
[2] *Department of Applied Mathematics, University of Leeds, Woodhouse Lane, Leeds LS2 9JT, UK*

arXiv:1407.6579v1 [astro-ph.GA] 24 Jul 2014

Accepted ... Received ...; in original form ...

ABSTRACT

We present 2D adiabatic magnetohydrodynamic (MHD) simulations of a shock interacting with groups of two or three cylindrical clouds. We study how the presence of a nearby cloud influences the dynamics of this interaction, and explore the resulting differences and similarities in the evolution of each cloud. The understanding gained from this small-scale study will help to interpret the behaviour of systems with many 10's or 100's of clouds.

We observe a wide variety of behaviour in the interactions studied, which is dependent on the initial positions of the clouds and the orientation and strength of the magnetic field. We find: i) some clouds are stretched along their field-lines, whereas others are confined by their field-lines; ii) upstream clouds may accelerate past downstream clouds (though magnetic tension can prevent this); iii) clouds may also change their relative positions transverse to the direction of shock propagation as they "slingshot" past each other; iv) downstream clouds may be offered some protection from the oncoming flow as a result of being in the lee of an upstream cloud; v) the cycle of cloud compression and re-expansion is generally weaker when there are nearby neighbouring clouds; vi) the plasma β in cloud material can vary rapidly as clouds collide with one another, but low values of β are always transitory.

This work is relevant to studies of multi-phase regions, where fast, low-density gas interacts with dense clouds, such as in circumstellar bubbles, supernova remnants, superbubbles and galactic winds.

Key words: hydrodynamics – ISM: clouds – ISM: kinematics and dynamics – shock waves – supernova remnants – turbulence

1 INTRODUCTION

The interstellar medium (ISM) is recognized to be highly dynamic. At any given time a substantial quantity of gas is found to be transitting between several different phases of thermal equilibrium. Such transitions are driven by a variety of heating and cooling mechanisms. Heating is dominated by vigorous energy input from high-mass stars, including their intense ionizing radiation fields, their powerful winds, and their terminal supernova explosions. Heating also occurs via the conversion of gravitational potential energy and from the impact of extragalactic material. Cooling is achieved via a multitude of radiative processes and through adiabatic expansion.

Given these conditions, it is not uncommon for hot, high speed material to interact with cooler, dense material (often referred to as clouds). Knowledge of the dynamical and thermal behaviour of gas in such interactions is necessary for a complete understanding of the nature of the ISM. For instance, in starburst galaxies, the energy input from high-mass stars inflates superbubbles which can burst out of their host. However, the properties of such flows may be controlled by their interaction with small clouds which dominate the mass in such regions. These clouds may be destroyed and their mass incorporated into the hot phase, a process known as "mass-loading". This behaviour is a key ingredient in models of galaxy formation and evolution (e.g., Sales et al. 2010), but is currently not calculated self-consistently in them. On the other hand, the compression of clouds by the flow may ultimately trigger new star formation.

By far the best studied case is that of a shock hitting an isolated spherical cloud. The hydrodynamics of the interaction have been reported in a number of papers in which the cloud density contrast, χ, and the shock Mach number, M, have been varied (e.g., Stone & Norman 1992,

⋆ E-mail: js07ra@leeds.ac.uk

Klein et al. 1994, Nakamura et al. 2006). The effect of other processes in this interaction have also been studied, such as magnetic fields (e.g., Mac Low et al. 1994, Shin et al. 2008), radiative cooling (e.g., Mellema et al. 2002, Fragile et al. 2004, Yirak et al. 2010), and thermal conduction (e.g., Orlando et al. 2005, Orlando et al. 2008). The turbulent nature of the destruction of clouds has been investigated too (e.g., Pittard et al. 2009, Pittard et al. 2010). In the purely hydrodynamic case clouds are destroyed via the growth of Kelvin-Helmholtz (KH) and Rayleigh-Taylor (RT) instabilities. The interaction becomes milder at lower shock Mach numbers, with the most marked differences occuring when the post-shock gas is subsonic with respect to the cloud. Cloud density contrasts $\chi \gtrsim 10^3$ are required for material stripped off the cloud to form a long "tail-like" feature. Efficient cooling causes the cloud to fragment.

The presence of magnetic fields can strongly affect the interaction. In 2D axisymmetry, magnetic fields parallel to the shock normal suppress Richtmyer-Meshkov (RM) and KH instabilities, and reduce mixing. The magnetic field is amplified behind the cloud due to shock focussing and forms a "flux rope" (Mac Low et al. 1994). In contrast, in 3D simulations with strong fields perpendicular or oblique to the shock normal the shocked cloud becomes sheet-like at late times, and oriented parallel to the postshock field. The cloud then fragments into vertical or near-vertical columns (Shin et al. 2008). More recent work including magnetic fields, anisotropic thermal conduction and radiative cooling of 3D shock-cloud interactions finds that intermediate strength fields are most effective at producing long-lasting density fragments - stronger fields prevent compression while weak fields do not sufficiently insulate the cloud to allow efficient cooling (e.g., Johansson & Ziegler 2013).

Relatively few investigations of the interaction of a flow with multiple clouds exist. The response of a clumpy and magnetized medium to a source of high pressure was considered by Elmegreen 1988, who derived jump conditions for cloud collision fronts under a continuum approximation. This work was extended using a multi-fluid formalism by Williams & Dyson 2002, who showed that shocks can rapidly broaden and thus create a more benign environment which aids the survival of multiphase structure passing through the shock.

Simulations in which the interaction of a flow over numerous obstacles is studied in detail are only just becoming feasible. However, it is clear that the flow responds differently to the presence of a group of clouds, with a global bow shock forming when the clouds are relatively close (e.g., Poludnenko et al. 2002, Pittard et al. 2005, Alūzas et al. 2012 - hereafter Paper I). The degree to which the nature of the flow changes depends on the relative amount of mass added to the flow by destruction of the clouds, i.e. the mass-loading factor. Simulations extending Poludnenko's work to higher mass-loading factors were presented by Paper I. This work found that the global flow is not strongly affected by the presence of clouds with density contrasts of $\chi = 10^2$, as it evolves similarly to a region of equivalent, uniform density. However, significant changes arise when the cloud density contrast increases to $\chi = 10^3$. In this case the total mass in the clouds becomes dominant at a much lower volume fraction (equivalently a lower total cross-section of the clouds). The resulting interaction does not affect the structure of the shock much, but significantly mass-loads the post-shock flow. This ongoing mass-loading of the flow as the clouds are destroyed can cause the shock to decelerate even after it has left the clumpy region.

The evolution of a cloud also changes when additional clouds are nearby. In isolation, clouds lose most of their mass through KH instabilites, with the largest scale instabilities taking some time to grow. In mass-loaded flows, instabilities develop more easily due to the turbulent nature of the flow. Clouds are also ablated more quickly due to the higher density of the mass-loaded post-shock flow.

Fig. 19 in Paper I shows that the cloud lifetimes can be reduced by as much as 40%, compared to the single-cloud lifetime at the same resolution. However, we have since discovered a problem with our previous analysis which for computational reasons was conducted on low resolution single- and multi-cloud runs. The problem is that the development of KH instabilities is significantly slowed at lower resolution and clouds instead lose mass through direct ablation. The latter is a stronger effect in the multi-cloud simulations due to the higher density of the flow caused by material mixing into it from clouds further upstream. Thus our previous low-resolution simulations in Paper I were biased against the development of KH instabilities but not against direct ablation, leading us to erroneously conclude that clouds in multi-cloud runs have shorter lifetimes. We now find from a high-resolution comparison of the lifetime of clouds in single- and multi-cloud simulations that the clouds are destroyed in essentially the same time[1].

MHD studies of the interaction of a shock with a single-cloud show that the field is amplified not so much in the shear layers and vortices but rather in regions of compression: ahead of the cloud for perpendicular shocks where field lines bunch up, and in a "flux rope" behind the cloud where the flow converges for the parallel-shock case (Mac Low et al. 1994). These simulations show that magnetic fields limit mixing and fragmentation, but do not stop it completely, and provide support to the cloud perpendicular to the field lines. Our goal in this paper is to determine the degree to which neighbouring clouds change this picture. In particular, we are interested in the amplification of the magnetic field and the presence of magnetically dominated regions with $\beta < 1$. Can clouds present in regions of enhanced magentic field enhance the field further or does it saturate?

[1] However, the nature of the destruction is a little different. In multi-cloud simulations, clouds initially lose mass a little more slowly than in single-cloud simulations because of the reduction in the shock-speed brought about by the mass-loading of the flow. However, as the shocked cloud moves further downstream it encounters increasing post-shock density relative to the single-cloud case, and this increases the rate of ablation slightly. The net effect is that the overall lifetime of the cloud is very similar to the single cloud case. Having said this, clouds with a higher density contrast than the majority of neighbouring clouds *do* seem to still be destroyed more quickly than their single-cloud counterparts. We tentatively suggest this is because of the dense shell of ablated material which overruns them and increases their rate of mass-loss from ablation (all similar clouds are destroyed by one cloud destruction length ($1L_{CD}$) behind the shock front, and so are not affected by the shell, whereas the denser clouds still exist at the time they are overrun by the shell). This effect will be investigated in a forthcoming paper.

Because of the complex nature of the interaction and the many free parameters which now also include the positions and separations of clouds, we limit this current study to interactions involving two or three clouds. For computational reasons we also limit our study to 2D (i.e. our clouds are infinite cylinders). This work will serve as a basis for future work exploring the interaction of a shock with many 10's and 100's of clouds in 2D and 3D.

The outline of this paper is as follows. In Sec. 2 we introduce our numerical method. Sec. 3 details the results of our simulations. In Sec. 4 we summarize and conclude.

2 METHOD

The computations were performed using the MG adaptive mesh refinement (AMR) code. The ideal magnetohydrodynamic (MHD) equations are solved using a linear Riemann solver for most cases and an exact solver when there is a large difference between the two states (Falle et al. 1998). Piecewise linear cell interpolation is used. The scheme is second order accurate in space and time, and is supplemented by a divergence cleaning technique described in Dedner et al. (2002).

The simulations were performed on 2D XY-cartesian grids, so that the clouds are actually infinite cylinders. Two grids (G^0 and G^1) cover the entire domain. Finer grids are added where they were needed and removed where they are not. Refinement and derefinement are controlled by differences in the solutions on the coarser grids with a tolerance of 1 per cent in the conserved quantities specified. Each refinement level increased the resolution in all directions by a factor of 2. The time-step on grid G^n is $\Delta t_0/2n$ where Δt_0 was the time-step on G^0. Refinement is performed on a cell-by-cell basis rather than patches.

A typical grid extended $X \in [-50 : 190]\, r_{cl}$ and $Y \in [-50 : 50]\, r_{cl}$, where r_{cl} is the cloud radius (identical clouds are assumed). Inflow boundary conditions were used at the negative X boundary, being set by the shock jump conditions. Free inflow/outflow conditions were used at the other three boundaries. Simulations were performed with two sets of resolutions: 32 cells per cloud radius (R_{32}), and 128 cells per cloud radius (R_{128}). The lower resolution runs used 7 grid levels, with $\Delta x = 2\, r_{cl}$ on the G^0 grid, while the higher resolution simulations used 8 grid levels, with $\Delta x = 1\, r_{cl}$ on the G^0 grid.

The simulations set up two or three clouds with a cloud density contrast of $\chi = 100$ and with soft edges following the density profile as specified in Pittard et al. (2009) with $p_1 = 10$. In all simulations the sonic Mach number of the shock was 3. The strength of the magnetic field and its orientation to the shock was varied. Values for the Alfvénic Mach number, the pre-shock field angle and the plasma β in different regions are given in Table 1. A different advected scalar is used for each cloud to track the cloud material. The time is measured in units of the cloud crushing timescale, $t_{cc} = \chi^{1/2} r_{cl}/v_b$, where v_b is the shock velocity in the ambient medium. The bow-shock reaches the Y boundaries at around $7.5\, t_{cc}$ and the simulations are terminated shortly afterwards. Adiabatic behaviour is assumed with $\gamma = 5/3$.

Table 1. Summary of the magnetic field strength and orientation in the single- and multi-cloud simulations performed. The value of the plasma β in the pre-shock (i.e. β_0) and post-shock regions is also provided, as well as its approximate value in the bow-shock region.

			Value of β in each region		
Case name	B angle	M_a	pre-shock	post-shock	bow-shock
b15b1	15°	2.91	1.13	6.06	7.1
byb1	89.9°	2.91	1.13	1.25	1.2
byb5	89.9°	6.16	5.06	6.05	5.5
bxb1	0°	2.91	1.13	12.4	21
bxb0.5	0°	2.03	0.55	6.05	10.5

3 RESULTS

The collective interactions between a large number of clouds can be incredibly complex. To better understand them we begin by reviewing the basic behaviour of a shock striking an isolated, magnetized, cylindrical cloud. We then investigate the simplest of multiple cloud cases, that of two clouds, before applying the insight from the 2-cloud simulations to simulations with 3 clouds. Single-cloud simulations are named using the format *sc bAbB*, where the "*sc*" indicates that it is of a single-cloud, the "*A*" indicates the orientation of the field ("*x*", "*15*" and "*y*" indicate parallel, oblique and perpendicular shocks), and "*B*" indicates the value of the pre-shock plasma β. 2-cloud simulations are named using the format *s2wYoX bAbB* (or often using the shortened forms *wYoX* or *wYoX bAbB*). Similarly, 3-cloud simulations are named using the format *s3wRaθ bAbB* (again also with shortened versions). *wYoX* and *wRaθ* identify the relative positions of clouds, see Sec. 3.2 and Sec. 3.3 respectivley for further details.

3.1 Single-cloud interactions

3.1.1 Parallel shocks

We begin by reviewing the morphology of the 2D interaction of a shock with a single magnetized, cylindrical cloud. In the parallel field case a "flux-rope" forms directly behind the cloud: the flow converging behind the cloud compresses the field lines, thus increasing the magnetic pressure which prevents the post-shock flow from entering it (see Fig. 1a). As a result the "flux-rope" not only has a low plasma β, but it also has very low momentum. These two conditions ($\beta < 1$ and $\rho|\mathbf{u}| < 0.5 \times \rho_{ps}|\mathbf{u}_{ps}|$) specify the "flux-rope" region in the parallel field case, but can also be met in other field arrangements.

Another important feature in the flow are the "wings". This is a region or regions alongside the flux rope which delineates where the flow is stripping material away from the cloud. This region shows up in the magnetic field structure of simulations with parallel shocks as the reversal of the magnetic field. In general the "wings" are shielded from the momentum of the flow, although occasionally they may contain higher density fragments stripped off the upstream cloud.

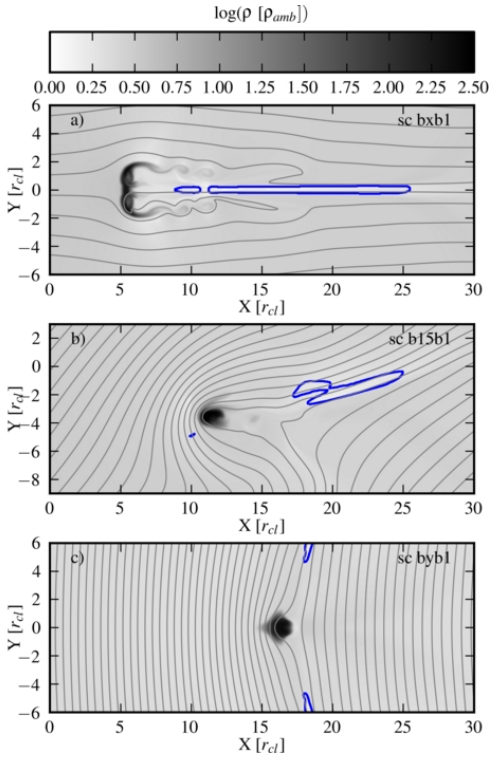

Figure 1. The morphology of interactions of a shock with a single cylindrical cloud. The calculations are in 2D, the sonic Mach number is 3 and the Alfvenic Mach number is 2.91 ($\beta_0 = 1.13$). The shock is a) parallel, b) oblique, and c) perpendicular . The cloud is initially positioned at the origin The grayscale shows the logarithmic density and magnetic field lines are also shown. The contour indicates regions with low plasma β and low momentum ($\beta < 1$ and $\rho|\mathbf{u}| < 0.5 \times \rho_{ps}|\mathbf{u}_{ps}|$). The time of the interaction is $t = 4\,t_{\rm cc}$.

3.1.2 Oblique shocks

In our oblique shock simulations a preshock field orientation of $\theta_0 = 15^\circ$ was chosen to be a representative oblique field case. This gives $\theta_{ps} = 45^\circ$ in the post-shock medium. When an oblique shock interacts with an isolated cylindrical cloud we find that the field lines wrap around the cloud keeping its cross-section roughly circular in shape (see Fig. 1b). Field lines above the cloud become nearly parallel to the direction of shock propagation[2] and some material is stripped off along them. Field lines below the cloud span a range of angles, with the region immediately upstream of the cloud having field lines nearly parallel to the shock front. Field amplification and "shielding" (i.e. where gas has minimal exposure to the ambient flow - e.g. gas in the lee of a cloud) now occur in distinct, but overlapping regions. The cloud is accelerated downstream and also laterally (in Fig. 1b) the cloud is seen to move to lower Y). The asymmetry of the cloud's motion reflects the asymmetric bunching and tensioning of the field lines and the direction of the postshock flow. Note that because the cloud in this simulation is actually an infinite cylinder field lines cannot easily slip past it. If the cloud were spherical we would expect some splitting and rearranging of the field, which could significantly change the forces acting on the cloud.

3.1.3 Perpendicular shocks

In the perpendicular field case, the magnetic field is initially amplified directly upstream of the cloud where the flow stagnates against it (see Fig. 1c). Because field lines cannot slip around the surface of the cloud (again due to its nature as an infinite cylinder), magnetic pressure and field tension continue to build with the result that the cloud accelerates rapidly downstream (compare the positions of the clouds in Fig. 1). This rapid acceleration acts to reduce the magnetic pressure and tension. Again we expect the evolution to be quite different to that of a spherical cloud.

3.2 Two-cloud interactions

We now investigate the interaction of magnetized shocks with 2 closely positioned clouds. We first examine the morphology of the interaction, and then discuss the acceleration of the clouds and the evolution of the plasma β. The 2-cloud arrangements are specified by their "width", which is the lateral distance between the cloud centers in units of the cloud radius (i.e. the separation of the clouds in the "y" direction), and by their "offset", which is the longitudinal distance between the clouds (i.e. their separation in the "x" direction). $t = 0$ is defined as the time that the shock reaches the leading edge of the more upstream of the two clouds.

3.2.1 Parallel shocks

In interactions with a parallel shock, the presence of a second cloud alongside the first cloud has the effect of suppressing the lateral re-expansion of the cloud. This is easily seen when comparing the single-cloud simulation *sc* and the 2-cloud simulation *w4o0* (in panels a) and b) of Fig. 2, respectively). The flow between the clouds is slowed and squeezed, but accelerates once past the clouds. The initial high pressure between the clouds drops due to the Bernoulli effect, causing the initial outwardly directed orientation of the flux-ropes to change towards an inwardly directed orientation[3].

As the initial position of one of the clouds is moved downstream the lateral suppression of the upstream cloud is reduced and it evolves more like the single cloud case. However, the downstream cloud is still much more affected by lateral confinement (see the results for *w4o8* shown in Fig. 2c).

The morphology of the downstream cloud is dependant on the "width" as well as the "offset", though the "width" is the dominant parameter. The simulations *w4o8*, *w2o8* and *w0o8* shown in panels c)-e) of Fig. 2 illustrate the diversity of the downstream cloud morphology, which we find can be categorised into three main types. When there is a sufficient gap between the clouds for the flow to weave through (e.g., as in simulation *w4o8* - see Fig. 2c), the downstream cloud is confined in a similar manner as if there was a cloud alongside it. In contrast, when a cloud is directly

[2] The postshock flow is about -7° to the shock normal.

[3] This behaviour is also seen in purely hydrodynamic simulations (Pittard et al. 2005).

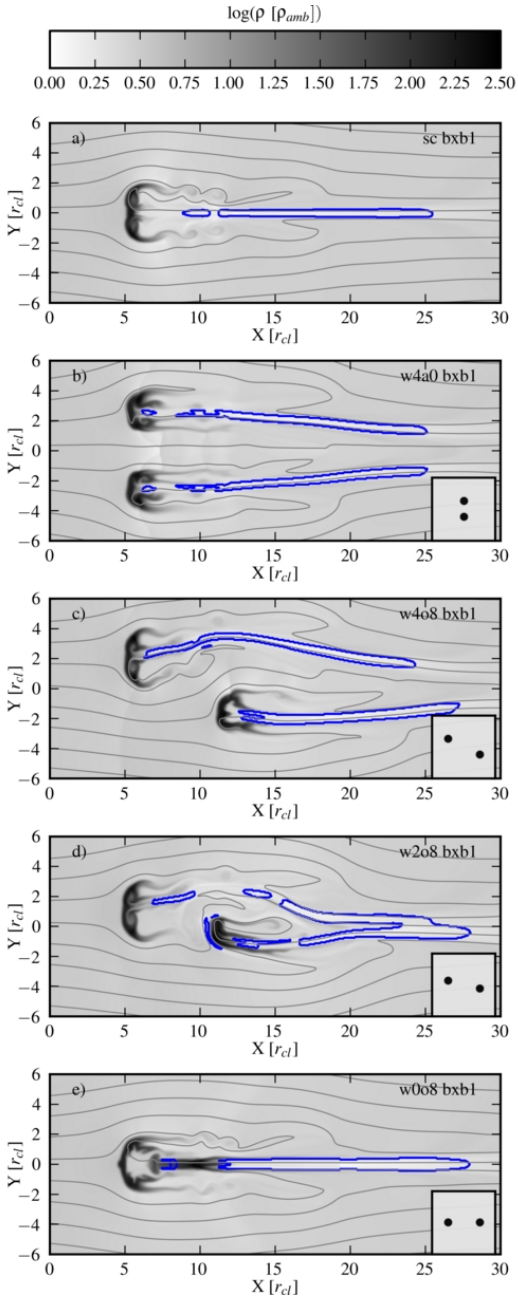

Figure 2. Snapshots of the morphology of a) an individual cloud and b)-e) 2-clouds with varying separation and offset at $t = 4\,t_{\rm cc}$. In all cases the magnetic field is parallel to the shock normal and $\beta_0 = 1.13$. The contour again shows the "flux rope" ($\beta < 1$ and $\rho|\mathbf{u}| < 0.5 \times \rho_{ps}|\mathbf{u}_{ps}|$), while the grayscale shows the logarithmic density. The 2-cloud simulations are identified by the initial "width" and "offset" of the clouds - the relative positions of the cloud at $t = 0$ are shown in the inset of each panel (shown at reduced scale). The resolution is R_{32}. At higher resolution the fine scale structure changes somewhat, but the general features of the flow and their dependence on the initial arrangement of the clouds remain unchanged.

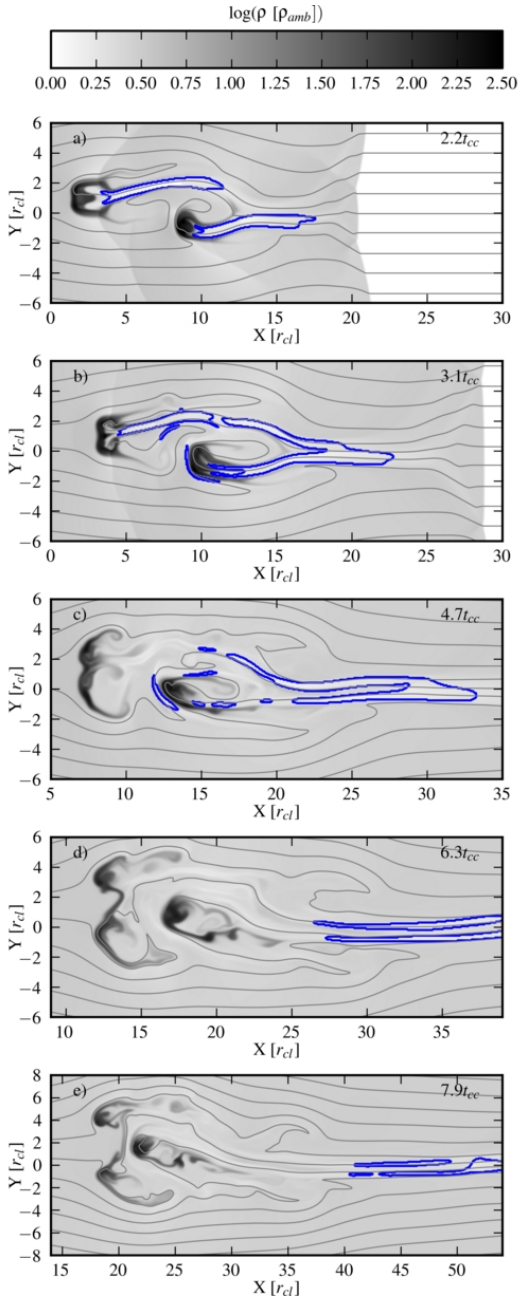

Figure 3. The time evolution of the 2-cloud simulation *s2w2o8* (the clouds are positioned with an initial "width" $= 2\,r_{cl}$ and "offset" $= 8\,r_{cl}$). The magnetic field is parallel to the shock normal and $\beta_0 = 1.13$. The logarithmic density and magnetic field evolution are shown at times $t = 2.2$, 3.1, 4.7, 6.3 and $7.9\,t_{cc}$ (top to bottom). The contour shows the "flux-rope" ($\beta < 1$ and $\rho|\mathbf{u}| < 0.5 \times \rho|\mathbf{u}|_{ps}$). In this simulation the downstream cloud is confined by the presence of the upstream cloud. Note the changes in the x- and y-coordinates in each panel.

behind an upstream cloud (e.g., as in simulation *w0o8* - see Fig. 2e), it falls in its "flux rope". The cloud is shielded from the flow and does not accelerate. The flow that tries to converge behind the upstream cloud (which forms the "flux rope") instead now converges on the downstream cloud, compressing it into an elongated shape. The upstream cloud

is also affected by the presence of the downstream cloud. As it accelerates towards the downstream cloud the tenuous gas between them is compressed, modifying the morphology of the upstream cloud in advance of their collision.

The third type of behaviour occurs when the downstream cloud is positioned such that it lies in the "wings" of the flow around the upstream cloud (e.g., see simulation *w2o8* - shown in panel d) of Fig. 2). To better understand the nature of this interaction we also show the time evolution of this simulation in Fig. 3. We find that the "flux ropes" of the two clouds merge downstream, while the magnetic field near the clouds becomes highly irregular. The latter is affected by the fact that the background flow becomes quite turbulent as it tries to force its way between the clouds at the same time as the clouds are distorted and influenced by the flow. The turbulent nature of the flow appears to be quite efficient at stripping material away from the downstream cloud. In spite of this, the cloud is mostly confined into an $r_{\rm cl}$-sized clump and does not spread very far along its fieldlines. Similar behaviour for the downstream cloud is also seen in simulation *w4o8* at late times as the upstream cloud expands and the downstream cloud is pushed into the shielded region.

3.2.2 Oblique shocks

We now study the interaction of an oblique shock with 2 cylindrical clouds. As the oblique magnetic field is not symmetric about the x-axis it provides another direction to supplement the "upstream" and the "downstream" designations. We define the "upfield" cloud as the one whose fieldlines encounter the shock front first. In the cases considered the upfield cloud is almost always the "top" cloud (i.e. has an initial positive "y" position). The exceptions are simulations *w2o-8* where the two clouds lie on roughly the same fieldlines, and *w2o-12* which was chosen specifically to have the "bottom" cloud as the "upfield" one.

Figs. 4 and 5 compare snapshots of the density and magnetic field structure of a single cloud case and a range of two cloud arranagements at $t = 4\,t_{cc}$. *Note that a negative "offset" signifies that the "top" cloud is the downstream one.* In all cases the field geometry causes the clouds to accelerate downwards (to more negative y positions) at the same time that they are accelerated downstream (to more positive x-positions). We see that the nature of the interaction is significantly modified by the presence of the second cloud, and that it depends on the relative initial positions of the clouds. In some cases the downstream cloud is protected from the oncoming flow by its position in the lee of the upstream cloud (e.g. as seen in simulation *w4o4* in Fig. 4, and in simulations *w4o8* and *w2o8* in Fig. 5). In other cases the downstream cloud feels the full fury of the oncoming flow (e.g., as seen for the top cloud in simulation *w4o-4* in Fig. 4 and simulation *w4o-8* in Fig. 5). Whether the top or bottom cloud accelerates fastest downstream depends on their relative orientation to the shock and the field (e.g., in simulation *w4o4* in Fig. 4 and in simulations *w4o8* and *w2o8* in Fig. 5 the top cloud accelerates fastest downstream, while in simulations *w4o-4* and *w2o-12* in Fig. 4 and simulations *w2o-8* and *w4o-8* in Fig. 5 the bottom cloud does so). Note that the bottom cloud in simulation *w0o8* shown in Fig. 5 is initially the upstream cloud.

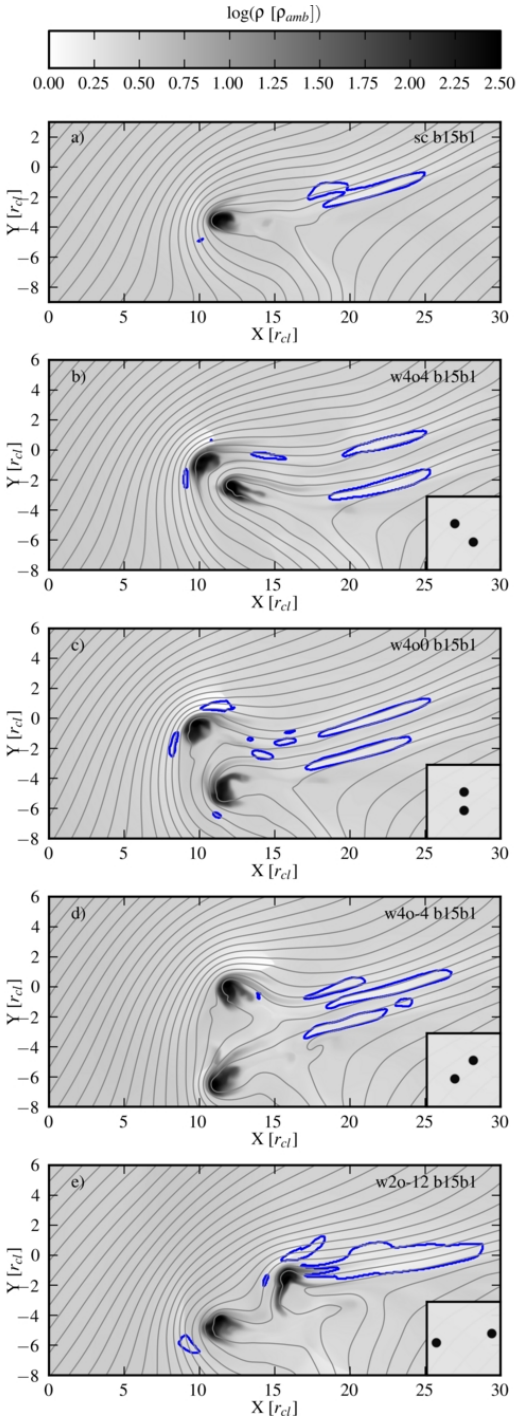

Figure 4. Snapshots at $t = 4\,t_{cc}$ of the morphology and field structure of shock-cloud simulations with an oblique magnetic field ($\theta_0 = 15°$ and $\beta_0 = 1.13$). The top panel shows the interaction with a single cylindrical cloud (*sc b15b1*), while the remaining panels show the interaction with two cylindrical clouds. The grayscale shows the logarithmic density while the contour shows the "flux rope".

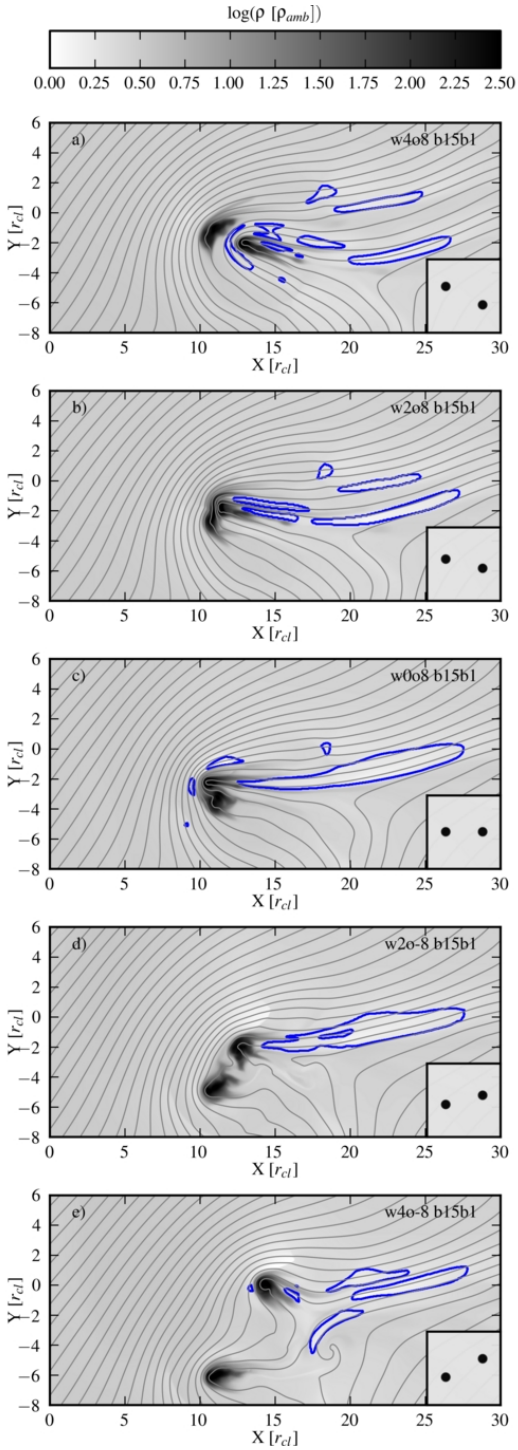

Figure 5. 2-cloud oblique-field snapshots like those in Fig. 4 but for a fixed cloud "offset" of $8\,r_{cl}$ and varied "width".

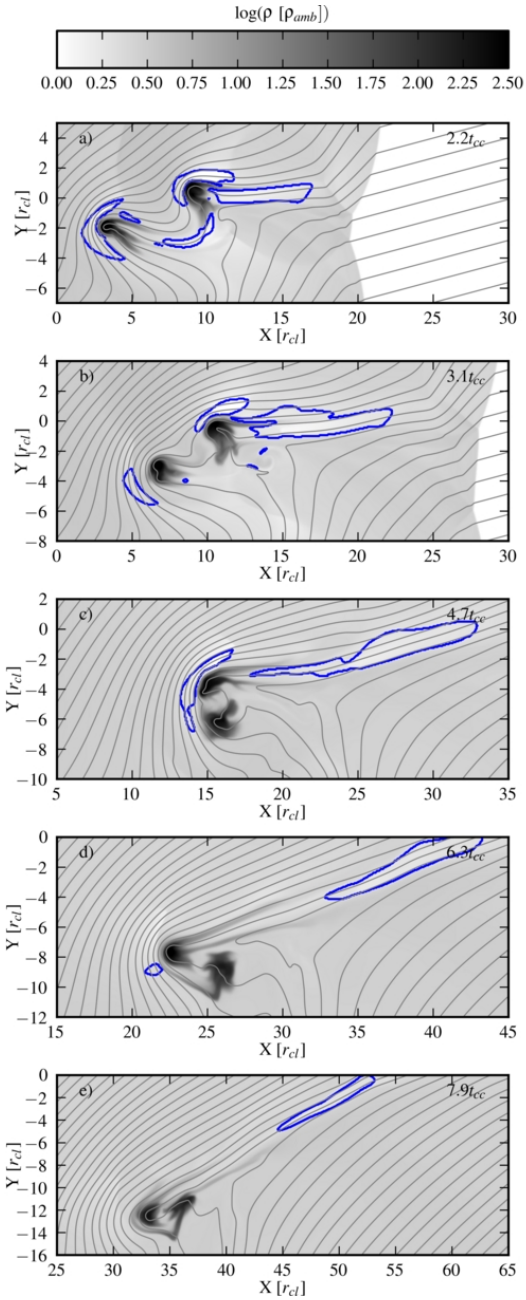

Figure 6. The evolution of the 2-cloud simulation *s2w2o-8* (the clouds are positioned with an initial "width" $= 2\,r_{cl}$ and "offset" $= -8\,r_{cl}$). The magnetic field is oblique to the shock normal ($\theta = 15°$ and $\beta_0 = 1.13$). The logarithmic density and magnetic field evolution are shown at times $t = 2.2$, 3.1, 4.7, 6.3 and $7.9\,t_{cc}$ (top to bottom). The contour shows the "flux-rope" ($\beta < 1$ and $\rho|\mathbf{u}| < 0.5 \times \rho|\mathbf{u}|_{ps}$). In this simulation the cloud which is initially upstream (i.e. the bottom cloud) is accelerated past the top cloud such that it becomes the most downstream cloud for $t \gtrsim 4.7\,t_{\rm cc}$.

Because the field lines are now forced to bend around two clouds, in many cases the region where the magnetic field is parallel to the direction of the shock propagation becomes larger and another region where the field is perpendicular extends between the two clouds (see, e.g., simulations *w4o4*, *w4o0* and *w4o-4* in Fig. 4). The clouds are also a lot less circular than compared to the case of a single cloud with an oblique field (compare any panel in Figs. 4 and 5 with panel a) in Fig. 4). Stripping now frequently occurs along multiple directions.

In many cases the wrapping of the field lines cause the top cloud to accelerated downwards (i.e. to more negative y positions) faster than the bottom cloud is accelerated in this direction. This can cause the clouds to either col-

lide or come as close together as allowed by the magnetic pressure which builds between them (see simulations *w4o8* and *w2o8* in Fig. 5). In other cases we find that the upstream cloud can become the most downstream cloud as the interaction evolves. Fig. 6 shows a time sequence from simulation *w2o-8b15b1* which shows how the upstream cloud (in this case the bottom cloud) overtakes the downstream (top) cloud. Once the bottom cloud moves into the "lee" of the top cloud it experiences reduced confinement forces and begins to diffuse. Simultaneously the top cloud becomes more exposed to the oncoming flow and experiences another episode of compression. This type of behaviour is seen in a large range of oblique simulations.

3.2.3 Perpendicular shocks

Finally, we study the interaction of a perpendicular shock with two cylindrical clouds. Figs. 7 and 8 compare snapshots of the density and magnetic field structure of interactions of a single cloud and 2 clouds with a perpendicular shock at $t = 4\,t_{\rm cc}$. In Fig. 7 the plasma β of the pre-shock medium is $\beta_0 = 5.06$, whereas the field is significantly stronger in Fig. 8 ($\beta_0 = 1.13$). As the field strength increases the magnetic field increasingly controls the dynamics of the interaction. This is evident from the suppressed instabilities and cloud mixing, enhanced diffusion of the cloud along the field lines, greater accceleration of the clouds downstream, and straighter field lines in Fig. 8 versus Fig. 7.

We again find that the presence of a second cloud has a major influence on the nature of the interaction. As the field lines wrap around the two clouds they are driven towards each other very rapidly. If clouds lie on the same field line they merge into a single clump (see the time evolution of simulations *w4o0* in Figs. 9 and 10). During this process a large continuous region of high magnetic pressure forms upstream of the clouds. Comparison of Figs. 9 and 10 reveals that there is some numerical diffusion present in the R_{32} simulations but that the same general behaviour occurs[4]. If the clouds do not lie on the same field line then a build up in the magnetic pressure between the clouds prevents their merger (see simulation *w4o8* in Fig. 7 where the contour between the clouds highlights the region of high magnetic pressure). Lazarian (2013) argues that the actual reconnection diffusion in turbulent plasmas might be quite fast and there might be a resemblance between numerical diffusion and magnetic reconnection in turbulent flows.

If the clouds are aligned or nearly-aligned with the direction of shock propagation the downstream cloud is shielded from the oncoming flow by the upstream cloud which moves very close towards it (see simulations *w2o8* and *w0o8* in Fig. 7). In such cases, the magnetic field lines between the clouds prevent the clouds from merging. The downstream cloud is compressed laterally by the upstream cloud which wraps around it.

[4] Due to this difference in numerical diffusion we find that the degree to which clouds merge when they do not lie on the same field lines is dependent on the resolution, with higher resolution simulations better able to prevent mixing and maintain distinct clouds in such cases (stronger fields also tend to keep clouds separate). R_{128} resolution is also necessary for accurate calculation of the plasma β in some circumstances - see Sec. 3.2.5.

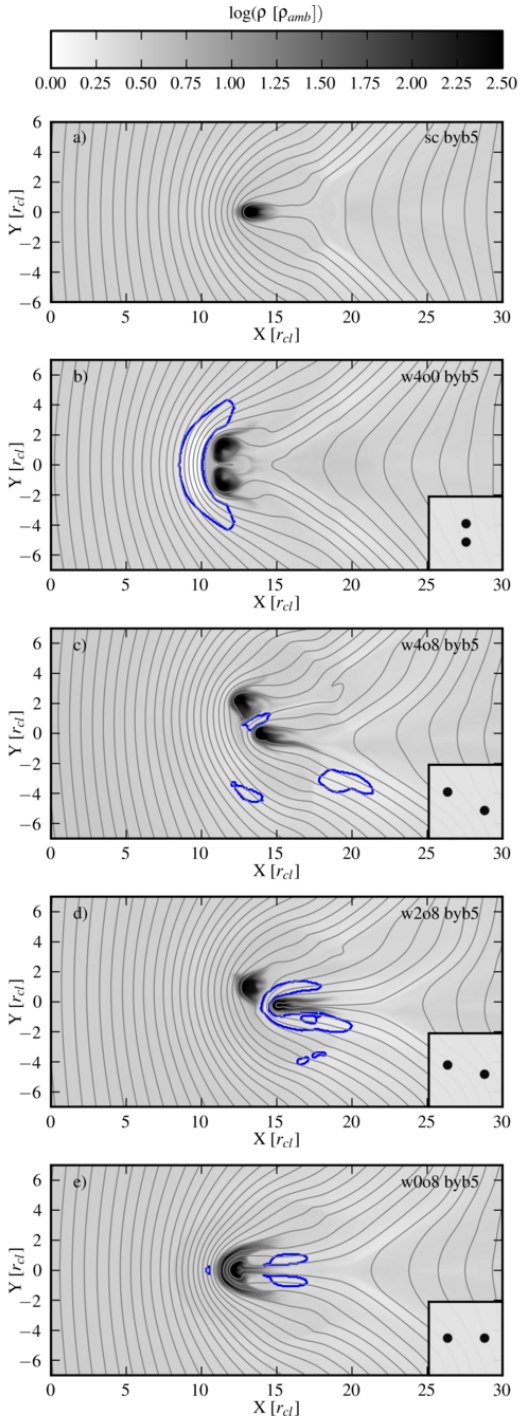

Figure 7. As Fig. 4 but with perpendicular magnetic fields and $\beta_0 = 5.06$. The time of each snapshot is again $t = 4\,t_{\rm cc}$.

In some cases, clouds which are initially separated quite widely can be driven towards each other to end up in a very compact arrangement. This behaviour is shown in Fig. 11, which shows the evolution of the interaction in simulation *w4o4*. In such cases, shock compression of the field lines naturally reduces the "offset" between the clouds, while their "width" is easily reduced by their motion along the field lines. In this example the downstream cloud moves towards the low pressure region behind the upstream cloud

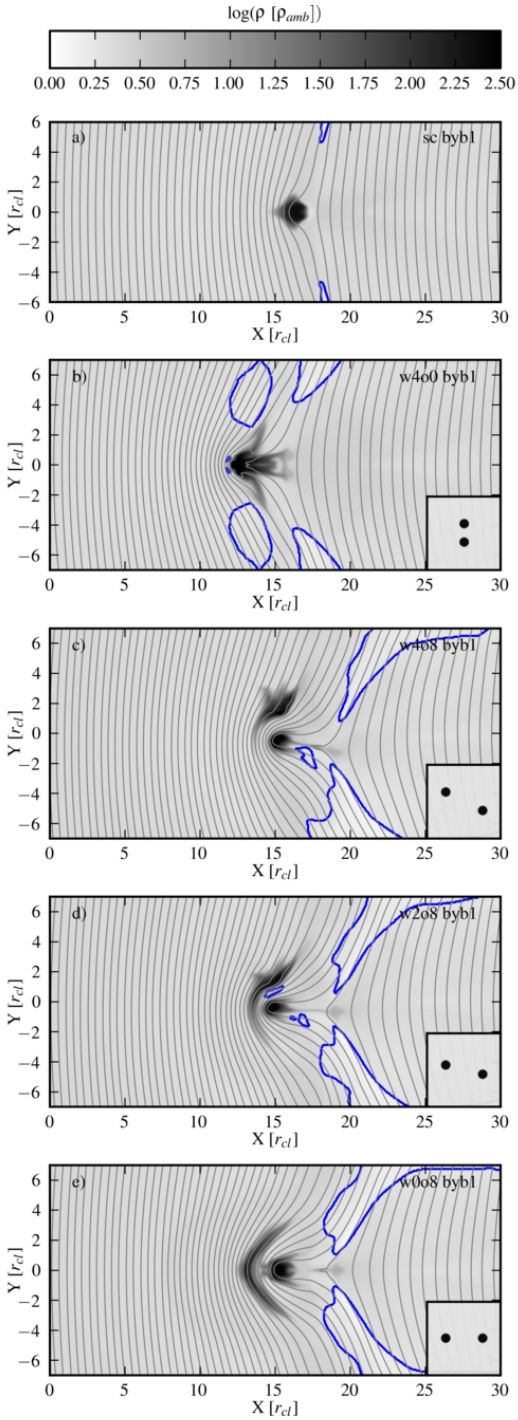

Figure 8. As Fig. 7 but with $\beta_0 = 1.13$. The time of each snapshot is again $t = 4\,t_{\rm cc}$. The stronger magnetic field now controls the dynamics more compared to the simulations shown in Fig. 7.

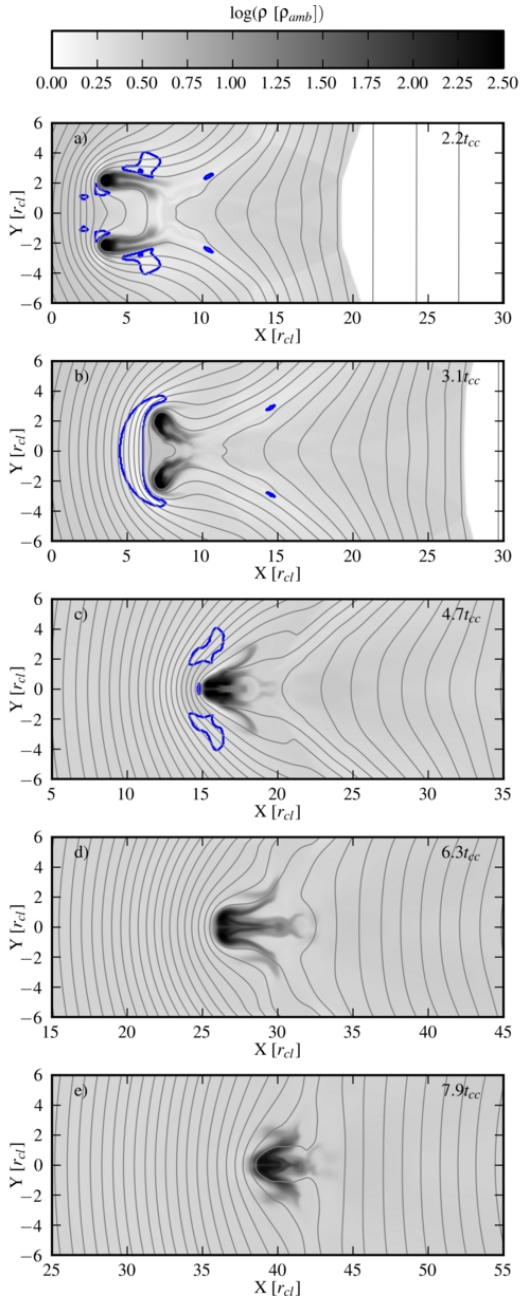

Figure 9. The time evolution of the 2-cloud simulation *w4o0_byb5* (the clouds are positioned with an initial "width" $= 4\,r_{\rm cl}$ and "offset" $= 0\,r_{\rm cl}$) The magnetic field is perpendicular to the shock normal ($\beta_0 = 5.06$). The logarithmic density and magnetic field evolution are shown at times 2.2, 3.1, 4.7, 6.3 and $7.9\,t_{\rm cc}$ (top to bottom). The contour shows the "flux-rope" ($\beta < 1$ and $\rho|\mathbf{u}| < 0.5 \times \rho|\mathbf{u}|_{ps}$). See also the second panel in Fig. 7.

and away from the high (magnetic) pressure region around the outside edge of the combined clouds. The field lines between the clouds prevent complete merging in this instance.

3.2.4 Cloud velocities

In simulations with a parallel or perpendicular magnetic field the clouds generally develop a small y-component to their velocity which often draws the clouds towards each other (see, e.g., simulation *w2o8* in Fig. 3 and simulation *w4o4_byb5* in Fig. 11).

However, the velocity evolution of a cloud is generally far more significant when the magnetic field is oblique. A clear and systematic distinction between the x-velocity component of the "top" and "bottom" clouds can be seen in Fig. 12. The "upstream" cloud accelerates first which is the

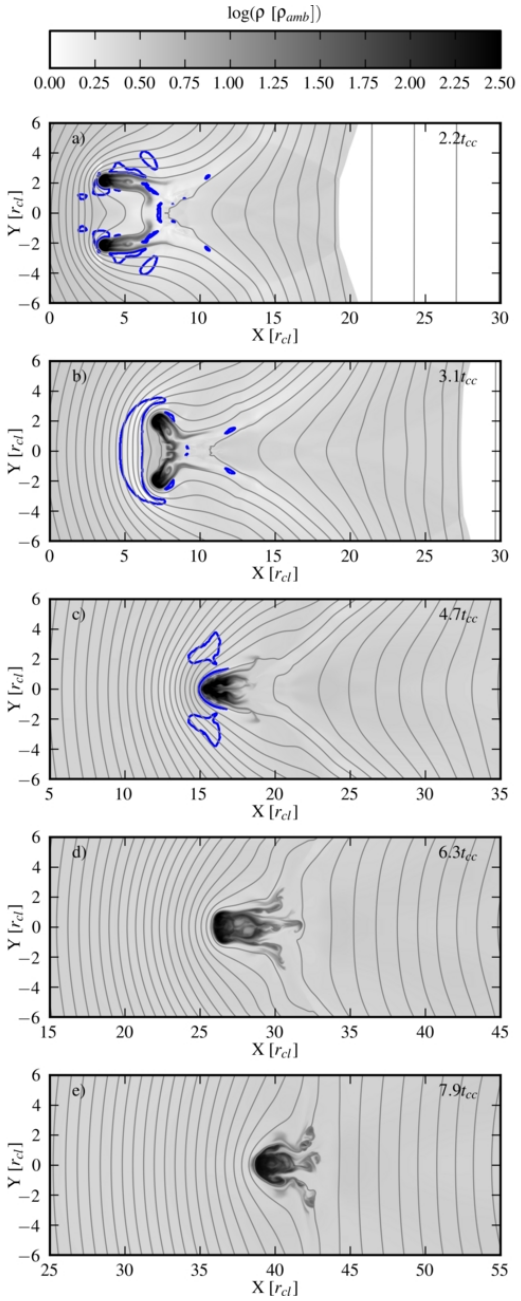

Figure 10. As Fig. 9 but with a resolution of 128 cells per cloud radius (instead of 32).

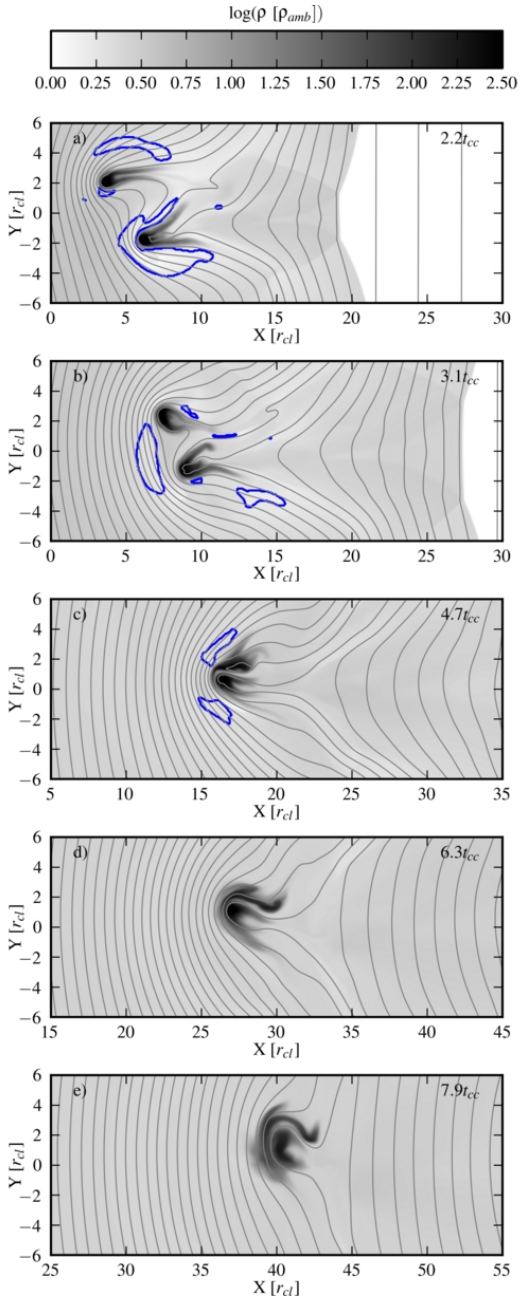

Figure 11. The time evolution of the 2-cloud simulation *w4o4_byb5* (the clouds are positioned with an initial "width" $= 4\,r_{\rm cl}$ and "offset" $= 4\,r_{\rm cl}$) The magnetic field is perpendicular to the shock normal ($\beta_0 = 5.06$). The logarithmic density and magnetic field evolution are shown at times $t = 2.2$, 3.1, 4.7, 6.3 and $7.9\,t_{\rm cc}$ (top to bottom). The contour shows the "flux-rope" ($\beta < 1$ and $\rho|\mathbf{u}| < 0.5 \times \rho|\mathbf{u}|_{ps}$). In this simulation the clouds accelerate towards each other with the upstream cloud eventually wrapping around the downstream cloud.

"top" cloud for positive "offset" and the "bottom" cloud if the "offset" is negative. Initially, the x-velocity in the "bottom" cloud grows at a rate similar to the isolated cloud case (compare the dotted lines for simulations *w4o-8*, *w4o4* and *w4o0* with the black crosses). The v_x velocity of each of these clouds overshoots slightly the post-shock flow value, as does the isolated cloud. In contrast, the acceleration of the "top" cloud is noteably slower after about $2.5\,t_{\rm cc}$ and in all simulations it reaches the post-shock flow value without any overshoot.

The bottom panel of Fig. 12 shows the evolution of the y-velocity component of the clouds. In the single cloud case the cloud significantly overshoots the velocity of the postshock flow which has a normalized value $v_y \approx -0.25\,c_{\rm s,0}$. The single cloud reaches its peak y-velocity of $\approx -0.8\,c_{\rm s,0}$ at $t \approx 7.5\,t_{\rm cc}$, before decelerating. At late times we would expect the cloud v_y to asymptote towards that of the post-shock flow but this clearly takes place on timescales in excess of $12\,t_{\rm cc}$. The y-velocity component of the clouds in the 2-

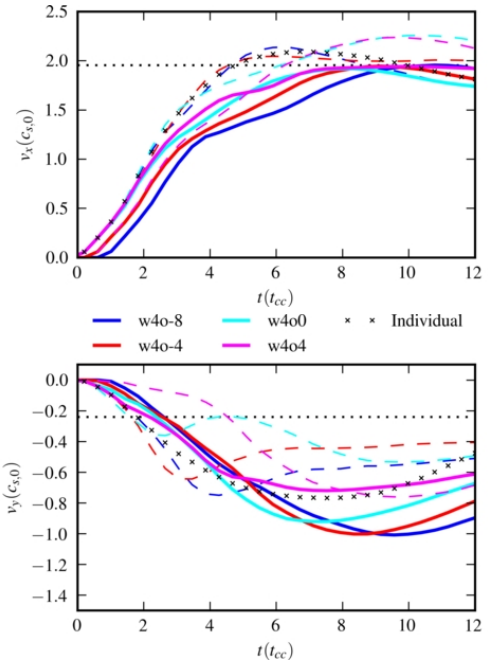

Figure 12. Evolution of the x- (top panel) and y- (bottom panel) cloud velocity components in simulations with 2 clouds and oblique magnetic fields. The velocity is normalized by the sound speed of the intercloud ambient medium. The initial "width" of the cloud distribution is identical in each simulation (being $4\,r_{cl}$), while the "offset" is varied. In each panel the "top" cloud in the distribution is shown using solid lines while dashed lines correspond to the "bottom" cloud. The dotted black line shows the intercloud velocity of the post-shock flow. Also shown is the velocity evolution of a single cloud simulation (indicated by the black crosses).

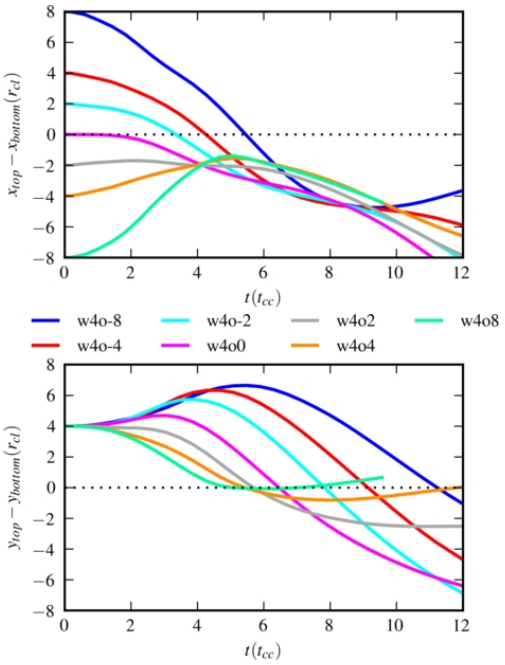

Figure 13. The evolution of the x- and y- separations of the clouds in 2-cloud simulations with oblique magnetic fields. A sign change (i.e. movement across the horizontal black line) represents a switch in relative position.

cloud simulations follows the same broad behaviour of initial acceleration, overshoot of the equilibrium value, and deceleration towards the postshock speed, but there are significant differences in the details. The "top" cloud accelerates downward slowly initially, but significantly overshoots the isolated cloud case later on (unless the "top" cloud is also the "upstream" one (e.g., *w4o4*), in which case its behaviour is closer to the isolated cloud). In contrast the "bottom" cloud initially accelerates faster than the isolated cloud, but starts slowing down much sooner (reaching a peak velocity of $\approx -0.65\,c_{s,0}$ at $t \approx 3\,t_{cc}$ for *w4o-4*). Simulation *w4o4* is again the exception - as the "downstream", "bottom" cloud is shielded from the flow it accelerates very slowly initially. Finally we note that some clouds (e.g., the "bottom" cloud in simulation *w4o0*) undergo a second period of acceleration.

Overall, we find that the "bottom" cloud moves faster in the "x" direction and the "top" cloud moves faster in the "y" direction. Thus if initially the "upstream" cloud is the "bottom" one then the upstream cloud will overtake the downstream cloud. This is highlighted in the top panel of Fig. 13 where we see that the clouds swap relative positions (i.e. cross the horizontal black line) in simulations *w4o-8*, *w4o-4*, *w4o-2* and *w4o-1*. It is also observed in simulation *w2o-8* as shown in Fig. 6.

However, we also find that the "top" and "bottom" clouds swap their relative y-positions in all of the simulations with "width" $= 4\,r_{cl}$ that we have investigated. This is shown in the lower panel of Fig. 13 where all the simulations cross the horizontal black line, irrespective of the initial "offset". We observe that a swap-over even occurs in simulations like *w4o-8*, where the "bottom" cloud is the first to accelerate and the separation between the clouds actually grows until $6\,t_{cc}$ (in this case the swap-over occurs at $t > 10\,t_{cc}$). Fig. 6 shows the swap-over process occuring in simulation *w2o-8* at $t \approx 8\,t_{cc}$ (here the "bottom" cloud moves underneath and then behind the "top" cloud).

3.2.5 The plasma β

Of the simulations performed, the parallel shock simulations with $\beta_0 = 1.13$ (i.e. models *bxb1*) have the highest postshock β (~ 12, see Table 1). It is in these simulations that instabilities are least suppressed by the magnetic field. Simulations with single clouds reveal that the results are sensitive to resolution, with a convergence study indicating that of order 100 cells per cloud radius are needed for accurate results (in keeping with previous work of adiabatic hydrodynamical shock-cloud interactions - see, e.g., Klein et al. 1994; Pittard et al. 2009). In contrast, the presence of additional clouds disturbs the flow such that longer wavelength instabilities play a more important role. This reduces the resolution requirements in multi-cloud simulations. However, in order to compare like-with-like, we perform the following analysis of β in the parallel shock simulations using resolution R_{128} for the multi-cloud simulations too.

We first study how the distribution of β in the simulations with a parallel shock changes as the initial positions of the clouds are varied. In each of the following figures we show the time evolution of the distribution of the plasma

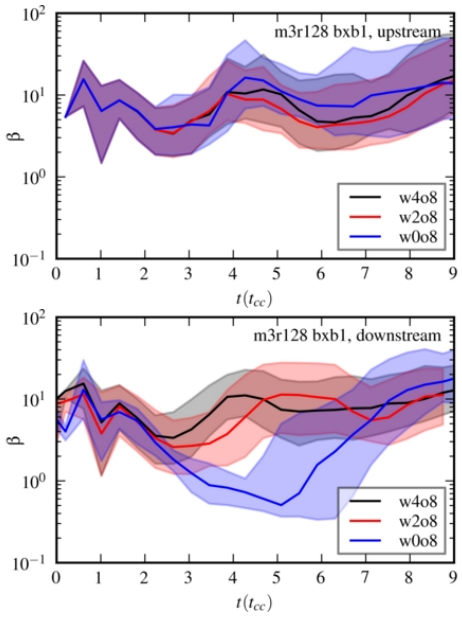

Figure 14. The time evolution of the β distributions for upstream (top panel) and downstream (bottom panel) clouds in R_{128} 2-cloud simulations with parallel magnetic fields and preshock $\beta_0 = 1.13$. The initial cloud "offset" is 8 while the initial cloud "width" is varied. The solid line shows the median β value and the area between the 25^{th} and 75^{th} percentiles is shaded.

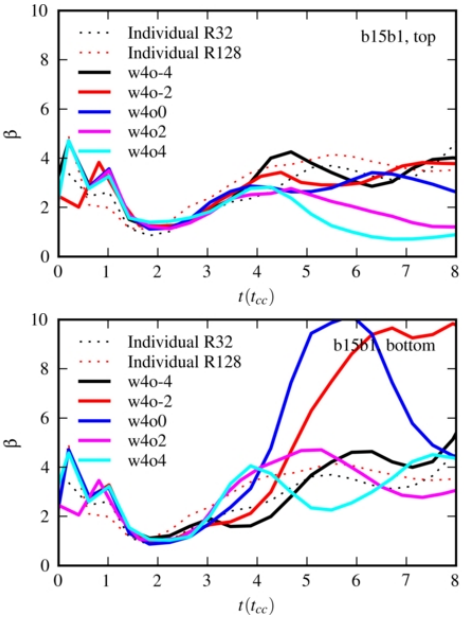

Figure 15. Evolution of the harmonic average of β in material from the "top" cloud (top panel) and the "bottom" cloud (bottom panel) in 2-cloud simulations with an oblique magnetic field (where $\beta_0 = 1.13$ and $\theta_0 = 15°$). The initial cloud positions have a "width" of $4\,r_{\rm cl}$ and varying "offset". The evolution of β in isolated clouds is also shown (for simulations with 32 (R_{32}) and 128 (R_{128}) cells per cloud radius).

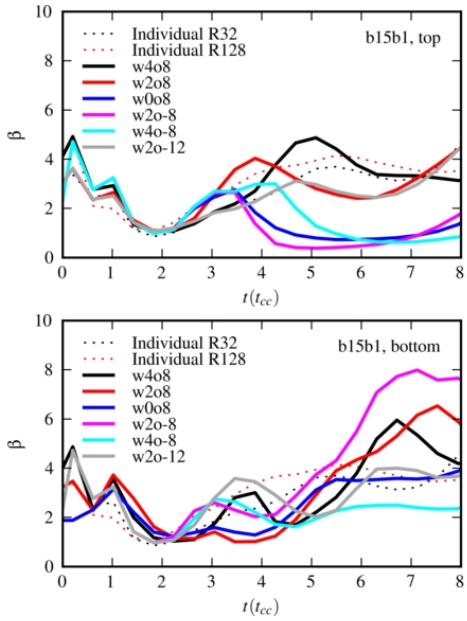

Figure 16. As Fig. 15 but for clouds in simulations with an initial "offset" of $8\,r_{\rm cl}$ and varying "width". The upstream cloud is identified as the "top" cloud in simulation *w0o8*.

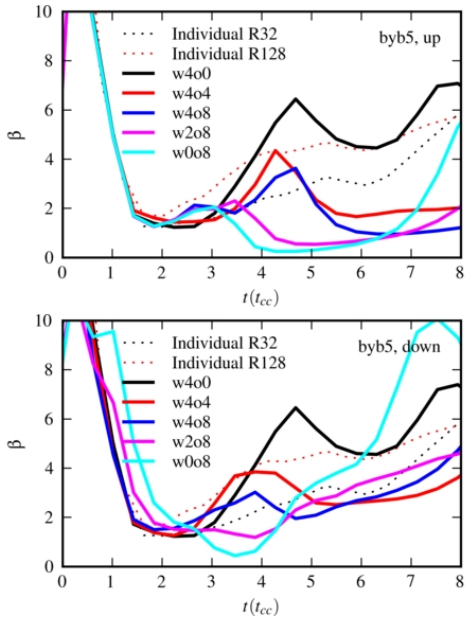

Figure 17. Evolution of the harmonic average of β in material from the upstream (top panel) and downstream (bottom panel) cloud in 2-cloud simulations with a perpendicular magnetic field ($\beta_0 = 5.06$). The evolution of β in isolated clouds is also shown (for simulations with 32 (R_{32}) and 128 (R_{128}) cells per cloud radius).

β of the cloud material (the distribution is calculated over all cells in the simulation upstream of the shock front but is weighted by the amount of cloud material in each cell). β changes with time as the cloud is first compressed, and then re-expands. At late times β should approach the value in the post-shock flow. This behaviour can be seen in Fig. 14.

We find that varying the initial cloud "offset" has no real effect on the β distributions when the initial cloud "width" is greater than the diameter of the clouds. In Fig. 14 we show how the evolution of β depends instead on the initial "width" of the cloud distribution for simulations with $\beta_0 = 1.13$. We find that the upstream cloud is not affected in the *w2o8* simulation, but the growth of β is delayed by $1\,t_{\rm cc}$ in the downstream cloud (compare the red and blue lines in the bottom panel of Fig. 14 between $3 \lesssim t/t_{\rm cc} \lesssim 5$). Note, though that this delay is not seen in the *bxb0.5* case where the magnetic field is more dominant.

In the *w0o8* case (see Fig. 2e)), the downstream cloud falls inside the flux rope and β drops to ~ 0.5 in the downstream cloud until the clouds collide. The beta distribution of the upstream cloud is also affected in this case - β is generally slightly higher due to the increased pressure downstream. The same behaviour is seen if the magnetic field is made slightly stronger. For example, in simulations with $\beta_0 = 0.55$ (models *bxb0.5*) the minimum β is still around 0.5 in the downstream cloud, while the increase of the plasma β in the upstream cloud is even more prominent.

We find that simulations with an oblique magnetic field are much less sensitive to resolution, and we are able to use simulations with a resolution of 32 cells per cloud radius. We adopt the harmonic mean as the average for the β statistics in these simulations: it demonstrates good convergence because it is not influenced by a small number of cells with high β where the flow is poorly resolved. The harmonic mean is thus a good estimator for the "typical" β value of cloud material, and it generally falls inbetween the $30^{\rm th}$ and $50^{\rm th}$ percentile values.

Figs. 15 and 16 show the evolution of the harmonic mean of β in material from the "top" and "bottom" clouds of various simulations. The "top" cloud is the upstream one if the "offset" is positive, and is the "upfield" cloud in all simulations except *w2o-12* and *w2o-8*. These figures also show the variation of β in simulations with a single individual cloud. In Fig. 15 we see the effect of varying the "offset" value of the initial cloud distribution while keeping the initial distribution "width" fixed at a value of $4\,r_{\rm cl}$. In contrast, in Fig. 16 the initial distribution "width" is varied while the "offset" is kept at 8 or $12 r_{cl}$.

These figures reveal that β is significantly reduced in the "top" cloud when it is the upstream one (see models *w4o2* and *w4o4* in Fig. 15, and models *w4o8*, *w2o8* and *w0o8* in Fig. 16). In model *w2o8* we see that $\beta < 1$ during the period $4 \lesssim t/t_{\rm cc} \lesssim 7$; Fig. 5 shows that the clouds collide at this time. In fact, the collision of the clouds is responsible for the low β values in the material of the top cloud in all of these simulations, and also in simulation *w0o8* (where low β values occur in the upstream cloud). In contrast, we find that β in material in the "bottom" cloud is similar to that in the isolated cloud or slightly higher.

When the "top" cloud is the "downstream" one, the harmonic mean of β in both of the clouds evolves similarly to the evolution of β in an isolated cloud. Exceptions to this behaviour occur only for the bottom cloud in simulations *w4o-2* and *w4o0* (see Fig. 15) and simulation *w2o-8* (see Fig. 16); in these cases the "bottom" cloud reaches much higher β values. The reason for this difference is evident from Fig. 6, which reveals that in simulation *w2o-8* the "bottom" cloud overtakes the "top" cloud and becomes the "downstream" cloud at the time when β starts growing. The same behaviour also occurs in the other two cases. For example, in simulation *w4o0* the bottom cloud crosses a line perpendicular to the upstream field lines passing through the "top" cloud at this time. Finally, we note that although the clouds also pass each other in *w4o-4*, this happens at a later time and greater separation with the result that β does not grow as much in the bottom cloud.

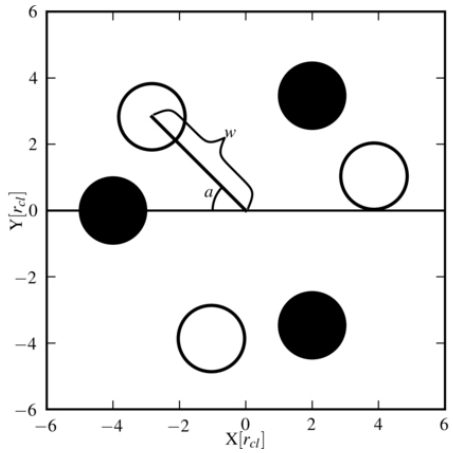

Figure 18. Illustrations of the cloud positions in 3-cloud simulations. Two particular arangements are shown: *s3w4a0* (with the clouds indicated by the filled circles) and *s3w4a45* (with the clouds indicated by the open circles).

Finally we study the evolution of β in simulations with a perpendicular magnetic field. The β in the post-shock flow of models *byb5* is 6.05. Since this is the same as in models *b15b1*, β in the shocked clouds varies in the range of $4 - 7$ for the majority of cloud arrangements in simulations with these field values.

The "upstream" clouds in simulations *byb5* correspond to "upstream"-"top" clouds in the oblique simulations *b15b1* and thus all such clouds have reduced β values (see models *w4o4*, *w4o8*, *w2o8* and *w0o8* in Fig. 17). We also find again that β in the downstream clouds evolves similarly to that in isolated clouds, and that only clouds that are shielded from the flow (such as the downstream clouds in simulations *w2o8* and *w0o8*) go through a phase of significantly reduced β (occuring at $t \approx 3 - 4\,t_{cc}$ in these cases). Because the clouds in simulation *w4o0* are on the same field line, β increases as they mix. An increase in β is also seen in the downstream cloud of *w0o8* but further examination indicates that it is principally due to mixing from numerical diffusion as this behaviour is not seen at higher resolution. Other higher resolution results track the lower resolution results almost exactly.

3.3 Three-cloud interactions

We now investigate the MHD interaction of a shock with 3 closely spaced clouds which are arranged to form the vertices of an equilateral triangle (see Fig. 18). The centroid of the triangle is located at the origin of the computational grid and the exact arrangement is defined by the angle between the vector to the most upstream cloud and the (negative) x-axis and the length of this vector (so dis-

tribution *w4a30* has the most upstream cloud located at $(x, y) = (-4 \times \cos 30^\circ, 4 \times \sin 30^\circ) = (-3.46, 2)$). The most upstream cloud is referred to as "cld1". The next cloud clockwise, referred to as "cld2", will be the one that is behind (directly or with some lateral offset) "cld1". The final cloud, "cld3", is then located off to the side.

A compact, *w4* arrangement gives a side length of $l = \sqrt{3} \times 4 = 6.93\, r_{cl}$ for the equilateral triangle. If considered as part of a hexagonal lattice this distribution would give a mass ratio (the ratio of mass in the clouds to the intercloud mass) $MR = 9.07$. A slightly wider *w8* arrangement (not considered in this work) gives $l = \sqrt{3} \times 8 = 13.86\, r_{cl}$ and $MR = 2.12$. The mass ratio can be increased by reducing w and by increasing the cloud density contrast, χ.

We now investigate the nature of the interaction with parallel, oblique and perpendicular shocks in turn.

3.3.1 Parallel shocks

The interaction of a shock with 3-clouds can be thought of as being similar to a 2-cloud scenario, but with the addition of a "modifier" cloud. Fig. 19 shows the nature of the interaction for a relatively compact arrangement of clouds. When clouds are placed further apart the morphology of the interaction increasingly resembles either *w4a0* or *w4a60*, except when the orientation is such that the clouds line up.

As with the previous 2-cloud simulations, the nature of the 3-cloud interaction depends on the relative positioning of the clouds. In Fig. 19a), we see that the "flux rope" from cld1 passes inbetween the two downstream clouds and completely detaches. In addition, an interesting low β, low momentum region forms near the inside "wing" of the downstream clouds. Rotating the cloud distribution to break the lateral symmetry we observe that the "flux ropes" of two of the clouds may merge (as seen in simulations *w4a15* and *w4a45* in Fig. 19b) and d). The merging of flux ropes was previously seen in the 2-cloud simulation *w2o8* shown in Fig. 2d). The location of the third cloud influences the sections of "flux rope" associated with individual clouds but the merged part looks the same. Finally, when cld2 falls directly into the "flux rope" of cld1 (as seen in simulation *w4a30* in Fig. 19c), the resulting "flux rope" appears very similar to that in the 2-cloud simulation *w0o8* shown in Fig. 2e), but the morphology of cld2 is significantly changed by the presence of the third cloud.

The time evolution of simulation *w4a15* is shown in Fig. 20. In this simulation the strongest interaction occurs between those clouds with the smallest difference in their lateral positions (cld1 and cld2 in this case). Compared to cld2, cld3 is able to retain a broadly symmetric structure for longer, with the only significant deviations by $t = 3\, t_{cc}$ being to its tail. After this time, cld3 becomes increasingly asymmetric in appearance. At $t = 6\, t_{cc}$, cld2 has a circular core and a tail of stripped material extending from its outside edge. Such a tail only occurs when a downstream cloud is in the "wings" of an upstream cloud.

To better understand the nature of the interactions between clouds in the 3-cloud simulations we now look at the evolution of the mass of the core region of each cloud and each cloud's density. We define cloud cores as circular regions with an average density $\langle \rho \rangle > \rho_{crit} = 120 \rho_{amb}$ (i.e. a 20% increase on the initial cloud density). Fig. 21 shows the evolution of the core mass in single-cloud simulations and in the 3-cloud simulations shown in Fig. 19. The core mass rises rapidly as each cloud is compressed and abruptly plateaus once 100% of the cloud material is above the density threshold. This takes roughly one cloud-crushing timescale by definition. Subsequent re-expansion of each cloud causes the core mass to decrease (in the single cloud case the core mass decreases to $\approx 0.5\, m_{\rm cl}$ by $t \approx 2\, t_{cc}$). In many cases the subsequent behaviour is oscillatory as the cloud cycles through phases of expansion and contraction, though a steady decline in the core mass is the dominant trend as material from the cloud mixes in with the ambient flow (ultimately the cloud density becomes equal to the post-shock density).

In many simulations the cloud fragments into multiple cores. When this happens the mass of the largest fragment is shown by the solid lines in Fig. 21 while the sum of the mass of all fragments is shown by the dotted lines. Any overlapping cores are merged into a single fragment. We find that this analysis is dependent on the resolution adopted in the simulations. As shown in the top panel of Fig. 21, a lower resolution simulation diverges from a higher resolution simulation at $t \approx 3\, t_{cc}$. Therefore we only consider high resolution runs in this analysis (differences due to the resolution can be delayed by choosing a lower density threshold, ρ_{crit}). In the high resolution single cloud case, the core splits into two fragments at $t \approx 5\, t_{cc}$, both of which dip below ρ_{crit} at $t \approx 6.5\, t_{cc}$ (causing the core mass shown in Fig. 21a) to drop to zero). Subsequent compression brings material above the density threshold again by $t \approx 7\, t_{cc}$.

Since cld1 is not downstream of any other cloud, it evolves similarly to an isolated cloud and fragments at $t \approx 4.5\, t_{cc}$ (see Fig. 21b). Fragmentation of cld1 is slightly suppressed in simulation *w4a60* because of the presence of the other clouds. alongside. However, subsequent oscillations in the core mass of cld1 due to expansion and contraction of the cloud appear to be much weaker compared to the single cloud case, indicating that the presence of the other clouds is again being felt. At $t = 9\, t_{cc}$, $0.4\, m_{cl}$ remains in the combined fragments of cld1. The exception to this is simulation *w4a30*, where the interaction of cld1 with cld2 pushes the average density of cld1 down to $70\, \rho_{amb}$ (i.e. below the density threshold for identification of material as "core"). The average density of cld1 in the other simulations is $\approx 90\, \rho_{amb}$ at this time, and for simulations with an isolated cloud it is at $\approx 100\, \rho_{amb}$.

Various types of interaction show up in the behaviour of the core mass of "cld2". Simulations *w4a0* and *w4a15* are noticeable for the large mass fraction which remains in the core and the lack of significant fragmentation. In both these simulations cld2 is on the "outside" edge of the distribution, and the average density of cld2 is similar to that of the single-cloud case. In contrast, the average density of cld2 is lower (and thus there is less mass above threshold) in simulations *w4a45* and *w4a60*. The cores also fragment in these cases. In these simulations cld2 is noteable for being in the "middle" of the cloud distributions. Fig. 19 shows that when cld2 is "outside" it is longer and narrower, whereas when it is in the "middle" it is wider and shorter.

Fig. 21 shows that the average core mass of cld3 at late times is similar to or slightly higher than that of an isolated cloud (note that the symmetry of simulation *w4a60* means that cld3 behaves identically to cld1, while the sym-

metry of simulation *w4a0* means that cld3 is identical to cld2). Very little fragmentation is seen in cld3 in any of the simulations, and in particular in simulation *w4a0* where cld2 is directly alongside it. In general the further downstream cld3 is, the more mass is contained in the core, though this variation is quite small and is somewhat time-dependent.

Fig. 22 shows the evolution of the density in cld2 in three of the 3-cloud simulations. We see that as various shocks pass through cld2 (the transmitted shock is the main one, but shocks also propagate inwards from the sides and back of the cloud), the average density increases by a factor of $3-4$. Reexpansion starts after $t \approx 1\,t_{\rm cc}$ and the density drops reaching a local minimum at $t \approx 2\,t_{\rm cc}$. The density then increases slightly due to compression from the ram pressure of the flow as the cloud is accelerated downstream. The density steadily decreases from $t \approx 3\,t_{\rm cc}$ as the acceleration subsides and as material is stripped away. In simulation *s3w4a30*, cld2 lies in the "flux rope" of cld1 and is largely shielded from the flow. As a consequence it does not experience a period of re-compression at $t \approx 3\,t_{\rm cc}$, but neither does it experience strong stripping by the flow. At $t \approx 4\,t_{\rm cc}$, cld1 collides with cld2 and the density of cld2 steadily increases up to $t = 9\,t_{\rm cc}$.

Fig. 23 shows that the evolution of β in the material of cld1 and cld3 is largely independent of the cloud arrangement. However, this is not the case for cld2, where clear differences can be seen between simulations in the second and third panels of Fig. 23. However, this is hardly surprising, since cld2 is variously located in the "flux rope" of cld1 in simulation *w4a30*, in the "wings" of cld1 in simulations *w4a15* and *w4a45*, in the "outside" flow in simulation *w4a0*, and in the "inside" flow in simulation *w4a60*. The presence of a third cloud appears to modify the behaviour seen in Fig. 14 - specifically β is higher when cld2 is between cld1 and cld3 (as in simulations *w4a45* and *w4a60*).

3.3.2 Oblique shocks

We now study the interaction of 3-cloud distributions with an oblique shock ($\theta_0 = 15^\circ$). Fig. 24 shows the resulting morphology at $t = 4\,t_{\rm cc}$. An additional simulation with a negative orientation angle is also included (simulation *w4a-30*). In the *w4a-30* and *w4a0* simulations, the modifier cloud is cld2[5], but otherwise it is cld3. A two stage process occurs: firstly, cld1 interacts (as in the 2-cloud case) with the nearest cloud along the flow, then these clouds jointly interact with the third cloud. For instance, simulation *w4a-30* in Fig. 24a) can be deconstructed as cld1 and cld3 interacting as in simulation *w0o8* in Fig. 5, and then the resulting combined "clump" interacting with cld2 as in simulation *w4o-4* in Fig. 4. Similarly, simulation *w4a60* in Fig. 24f) shows cld1 and cld2 interacting as in simulation *w4o4*, and then together interacting with cld3 as in simulation *w4o0* (compare Fig. 24a with Fig. 4d). The secondary interaction can also be categorised in terms of a "width" and an "offset". In the 3-cloud simulations studied, it appears that the appropriate width is the average "width" between the combined clump and the third cloud, while the appropriate offset is between the more upstream of the two clouds interacting in the first stage and the third cloud with which they interact in the second stage[6]. Note that the secondary interaction has a greater effective "width" than the 2-cloud cases considered in Sec. 3.2. This means that the separation at closest approach is greater and that a secondary collision between the combined clump and the third cloud does not occur. However, otherwise the morphologies are roughly equivalent.

Fig. 25 shows the time evolution of simulation *s3w4a-30* while Fig. 26 shows the time evolution of simulation *s3w4a45*. In simulation *s3w4a-30*, cld1 is initially at the bottom-left of the distribution, cld2 is at the top-right, and cld3 is at the bottom right (see also Fig. 24a). As the shock sweeps over, cld1 moves towards cld3 which is in the lee of cld1. cld1 engulfs cld3 by $t \sim 4\,t_{\rm cc}$, and cld3 is then confined by the magnetic field threaded through cld1. In contrast, cld2 evolves in a relatively isolated way. The flow tries to force its way between cld1/3 and cld2, but the field lines between these two regions prevent this. In contrast, in simulation *s3w4a45* cld1 is intitially at the top-left of the distribution, cld2 is the most downstream cloud, and cld3 is at the bottom left (see also Fig. 24e). Fig. 25 shows that cld1 and cld2 interact first, and that cld1 engulfs cld2. Although cld3 is initially upstream of cld2, cld3 lies downfield. Thus as the interaction proceeds, the tension in the field lines created by the flow causes cld3 to accelerate downstream faster than the other clouds.

In the oblique field case cld1 often has very low β at late times (see Fig. 27). Low β's at late times were previously seen in the top cloud of the 2-cloud simulations in Sec. 3.2 (see simulations *w4o8*, *w2o8* and *w0o8* in Fig. 16). In each case this is caused by the collision of the cloud with a cloud further downstream. Fig. 24 reveals that in the two cases where β stays higher (simulations *w4a15* and *w4a60*), cld1 has not collided with another cloud by $t = 4\,t_{\rm cc}$. In simulation *w4a15*, Fig. 24 shows cld1 about to squeeze between the two other clouds. cld1 proceeds to move into the "shadow" of cld2, and β in cld1 rapidly grows after $t = 6.5\,t_{cc}$. In simulation *w4a60*, cld1 and cld2 accelerate at a similar rate and do not collide (Fig. 24 shows these clouds still with significant separation at $t = 4\,t_{\rm cc}$). However, after $t = 6\,t_{\rm cc}$, as these clouds get close, β decreases in cld1.

The evolution of β in the other two clouds does not deviate much from the single-cloud case (see the middle and bottom panels of Fig. 27). The only noteworthy behaviour is that cld2 generally has a slightly lower β, while cld3 has a slightly higher β, at late times. β in cld2 is most different from the single-cloud case for simulation *w4a0* (β becomes very low by $t \gtrsim 7\,t_{\rm cc}$), while for cld3 it is simulation *w4a30* (β becomes very large at $t \gtrsim 5\,t_{\rm cc}$).

3.3.3 Perpendicular shocks

In this section we study the interaction of a perpendicular shock with 3 closely spaced cylindrical clouds. Fig. 28 illustrates the range of morphologies which exist at $t = 4\,t_{\rm cc}$ from a variety of simulations. It reveals that collisions are common. The collisions increase the density of the downstream cloud of the pair and in some cases can last up to $t \sim 10\,t_{cc}$ (cf. Fig. 29). In all cases the magnetic field in the oncoming

[5] Naively we expect the switch to happen at an angle $a \approx 5^\circ$.

[6] So it is possible to make a-priori estimates of these values.

flow is unable to pass between the clouds. It instead piles up at the upstream side and the field lines then bend around the clumpy region. Clouds either side of the center of the region then behave like the "top" cloud in the 2-cloud oblique simulations (cf. Sec. 3.2.2).

Fig. 29 shows the time evolution of simulation *s3w4a15*. cld1 is initially accelerated towards cld2 and cld3, and at $t = 4.6\,t_{\rm cc}$ it appears to be poised to squeeze between them. However, the snapshot at $t = 6.3\,t_{\rm cc}$ reveals that this does not happen. Instead, the field line that cld1 sits on is not able to force its way between cld2 and cld3, and cld1 ends up spreading along it while the field line instead wraps around cld2 and cld3. At the same time, cld2 and cld3 are forced together and mostly merge (they are on similar field lines). The level of mixing depends on the field strength and the degree of diffusion of material across the field lines. The field lines straighten out at later times as the clouds are accelerated up to the flow speed of the post-shock gas. It is clear that the overall "x"-size of the clumpy region is reduced by the field compression in this direction, while the "y"-size is reduced by the diffusion of clouds along the field lines.

Fig. 30 shows the evolution of β in the material of cld1, cld2, and cld3 in simulations with a perpendicular field ($\beta_0 = 5.06$). In general, we see that β in cld1 is much lower than the isoated single cloud case, except for simulation *s3w4a60*. This simulation is noteable because it is the only one in which cld1 is sufficiently on the "outside" of the distribution that it does not collide with any of the other clouds (see Fig. 28). Fig. 30 also shows that the β in cld2 is similar to but generally lower than the isolated cloud case. β is most variable in simulation *s3w4a30* (in cld2 it is low at $t = 3.5 - 4\,t_{\rm cc}$ when cld1 is compressing cld2, becomes noticeably higher at $t = 6\,t_{\rm cc}$, and then drops again afterwards as it interacts strongly with cld3). The value of β in cld3 shows the most difference between simulations. For *s3w4a0* it stays low for most of the simulation time, but for simulations *s3w4a15* and *s3w4a30* β becomes very high at $t \approx 6.5\,t_{\rm cc}$. Fig. 29 shows that in simulation *s3w4a15*, cld3 moves into the lee of cld1 at about this time (so is sheltered), but by $t = 7.9\,t_{\rm cc}$ cld1 has collided with it, decreasing β once more.

4 SUMMARY AND CONCLUSIONS

The results shown in Sec. 3 illustrate that the presence of nearby clouds modifies the evolution of a shocked cloud. In general, clouds on the same field lines are able to merge, even if they are quite widely separated. Conversely, clouds on different field lines tend to "rebound" from each other if they are squeezed closely together. However, the details of the simulations are complicated. We now summarize the main results and attempt to draw generalities where possible, commenting on parallel, oblique and perpendicular shock interactions in turn.

In the case of a parallel shock, the shocked cloud needs to push aside fieldlines in order to expand laterally and this is made more difficult by a cloud alongside. Hence the expansion and fragmentation of the cloud is reduced. The downstream cloud is not very sensitive to the distance along the direction of the shock normal to the upstream cloud, at least for the range studied ("offsets" $1 - 8\,r_{cl}$). Rather, for parallel shocks, the separation of clouds perpendicular to the shock normal (i.e. their "width") largely determines their evolution. As the field lines disturbed by the upstream cloud advect downstream, they curl round and confine any downstream cloud separated by "widths" $1 - 4\,r_{cl}$. At "widths" of $4\,r_{cl}$ the evolution of clouds is analogous to the evolution of clouds alongside one another (i.e. with an "offset"≈ 0). At a "width" of $2\,r_{cl}$, the downstream cloud is confined and roughly circular, with mass stripping occuring along a tail from its outside edge. Such clouds are pushed towards the lower pressure region behind the upstream cloud and start expanding once in the lee. At negligible "widths" a downstream cloud can fall in the "flux-rope" of the upstream cloud. While the initial shock compression of the downstream cloud is comparable to that of an isolated cloud, it is subsequently shielded from the flow and is not compressed nor accelerated significantly. After shock compression and re-expansion the properties of the downstream cloud are relatively constant until the upstream cloud ploughs into it (i.e. the evolution of a cloud in a flux rope is delayed until the upstream cloud reaches it).

In general, the presence of clouds downstream increases β in the upstream cloud via mechanical interaction, while clouds alongside decrease β by suppressing lateral expansion. By far the biggest effect is when a cloud is directly behind and in the "flux-rope" of an upstream cloud: in this case β in the downstream cloud can be significantly reduced for an extended period of time.

This basic behaviour also holds when a parallel shock interacts with three clouds, though the additional cloud modifies the morphology slightly. The additional cloud now allows a distinction to be made concerning whether the downstream cloud lies "inside" or "outside" with respect to the rest of the distribution (e.g., simulation *w4a15* vs. simulation *w4a45*). An outside cloud is confined much as in the 2-cloud simulations, but the field lines cannot curl as much around an inside cloud. The plasma β is generally higher in inside clouds, yet they are less confined than outside clouds.

The interaction of an oblique shock with clouds is a more general case than the specific cases of interactions of parallel or perpendicular shocks. With oblique shocks, as well as considering whether a cloud is upstream or downstream, one must also consider whether it is upfield or downfield. In 2-cloud interactions we see some interesting dynamics where the upstream cloud accelerates past the downstream cloud, and then swings into its lee. The "shielded" cloud then experiences reduced confinement forces and begins to diffuse, while the cloud more exposed to the oncoming flow experiences another period of compression. Clouds are given much faster transverse motions than those interacting with parallel or perpendicular shocks. The plasma β in the upstream cloud can drop below unity for a duration of a few $t_{\rm cc}$ when it collides with the downstream cloud. The interaction of an oblique shock with three clouds shows the same type of behaviour, and can be understood in terms of the interaction of the most upstream cloud with its nearest neighbour, and then their joint interaction with the remaining cloud.

The interaction of a perpendicular shock with clouds is again a more specific case. If the clouds are side-by-side they have a chance of merging. We clearly see this in simula-

tions where the clouds are separated with an initial "width" of $4\,r_{\rm cl}$, but as the width is increased the clouds should eventually evolve as isolated clouds. We have not explored the transition between these regimes, but it will certainly depend on paramters such as M, χ and β_0. When the clouds have a non-zero "offset" the fact that they exist on separate field lines prevents them from fully mixing. Nevertheless, the clouds tend to be driven towards each other much more strongly than when the shock is parallel or oblique. If the clouds have a small "width" and larger "offset" the upstream cloud tends to get driven into and then wraps around the downstream cloud. Like the oblique case, the plasma β in the upstream cloud can become less than unity when it collides with a downstream cloud. When three clouds are present, the most upstream or most downstream cloud may be prevented from moving between the other two clouds due to the tension in the field. Because the field lines also prevent the flow from passing between the clouds the magnetic field builds up on the upstream side and then bend around the clumpy region.

Previous work examining the MHD interaction of a shock with a single cloud found that the plasma β is low where the flow is compressed, rather than the magnetic field being turbulently amplified. The 2-cloud and 3-cloud interactions presented in this work are more turbulent than single-cloud interactions due to the presence of neighbouring clouds, but low values of β are still not seen very often. When they are, it is again mostly due to the compression of the field by the flow, and is ultimately transient in nature. This highlights the difficulty of obtaining regions of low β (e.g., $\beta < 1$) in adiabatic simulations. To obtain such regions it is probably necessary to invoke cooling to reduce the thermal pressure (e.g., van Loo et al. 2007, 2010). citeJohanssonZiegler2013 find that a weak perpendicular field ($\beta \sim 10^3$) is able to suppress conduction without limiting compression resulting in the highest density compressions of an individual cloud. Without considering the cooling, we find that moderate fields ($\beta = 5$) are effective at bringing several clouds together.

We note that the interaction of magnetized clouds has also been studied in solar physics, where Shen et al. 2012 modelled the propagation and collision of two coronal mass ejections (CMEs) in interplanetary space. The resulting structures and their evolution resemble some of the work shown in the present paper, though it is clear that additional complexities, such as magnetic reconnection in the neighbourhood of boundary layers (c.f. Chian & Muñoz 2012, occur. Reconnection in turbulent flows is discussed in Lazarian 2014).

We now offer some thoughts on some important questions concerning the ISM. At this stage it is difficult to say anything about diffuse cloud lifetimes because the clouds in the simulation are 2D instead of 3D and some important physical processes, such as cooling and conduction, were not included. However, it is clear that the lifetimes are affected by the environment around the cloud, and specifically the presence of nearby clouds which can affect the flow and field lines. We have not considered specific observables in this work (such as emission maps), so it is unclear what types of structures would actually be visible. We note that some other works which have focussed on observables have considered high velocity clouds (Shelton et al. 2012; Henley et al. 2012), supernova remnants (e.g., Patnaude & Fesen 2005; Obergaulinger et al. 2014), and galactic winds (e.g., Marcolini et al. 2005). These works indicate that it is possible to gain some insights into some of the key parameters, such as the interstellar magnetic field, the Mach number of the shock, the properties of the clumpy medium, and the nature of the pressure sources. Insight into such parameters is most forthcoming, of course, when specific sources are modelled.

The present study has illustrated some of the complexity inherent in MHD interactions of a shock with multiple clouds, and attempts to lay some of the necessary foundations for understanding this problem. In future work we will build on the present study to examine the MHD interaction of a shock with many tens and hundreds of clouds. We will also extend this work to spherical as opposed to cylindrical clouds. The interaction could be quite different between these two cases because field lines will be able to slip past spherical clouds, which could significantly change the forces acting on the clouds. In addition, there could be interesting interactions between clouds whose field lines lie in different planes. For instance, consider the interaction of a cloud in one plane with a second cloud in an adjacent parallel plane where there are different field lines in each plane. If the planes are far enough apart then the clouds should evolve independently (one plane might slip sideways relative to the other). However, the evolution may be markedly different when the planes are close enough together that pressure interactions occur between them.

ACKNOWLEDGEMENTS

We would like to thank the referee for a helpful report which improved this paper. JMP would like to thank the Royal Society for previously funding a University Research Fellowship and STFC for continued support.

REFERENCES

Alūzas, R., Pittard, J. M., Hartquist, T. W., Falle, S. A. E. G., & Langton, R. 2012, *MNRAS*, 425, 2212

Chian, A. C.-L., & Muñoz, P. R. 2012, in EAS Publications Series, Vol. 55, EAS Publications Series, ed. M. Faurobert, C. Fang, & T. Corbard, 327–334

Dedner, A., Kemm, F., Kröner, D., Munz, C.-D., Schnitzer, T., & Wesenberg, M. 2002, Journal of Computational Physics, 175, 645

Elmegreen, B. G. 1988, *ApJ*, 326, 616

Falle, S. A. E. G., Komissarov, S. S., & Joarder, P. 1998, *MNRAS*, 297, 265

Fragile, P. C., Murray, S. D., Anninos, P., & van Breugel, W. 2004, *ApJ*, 604, 74

Henley, D. B., Kwak, K., & Shelton, R. L. 2012, *ApJ*, 753, 58

Johansson, E. P. G., & Ziegler, U. 2013, *ApJ*, 766, 45

Klein, R. I., McKee, C. F., & Colella, P. 1994, *ApJ*, 420, 213

Lazarian, A. 2013, in Astronomical Society of the Pacific Conference Series, Vol. 474, Numerical Modeling of Space Plasma Flows (ASTRONUM2012), ed. N. V. Pogorelov, E. Audit, & G. P. Zank, 15

Lazarian, A. 2014, *Space Sci. Rev.*, 181, 1
Mac Low, M., McKee, C. F., Klein, R. I., Stone, J. M., & Norman, M. L. 1994, *ApJ*, 433, 757
Marcolini, A., Strickland, D. K., D'Ercole, A., Heckman, T. M., & Hoopes, C. G. 2005, *MNRAS*, 362, 626
Mellema, G., Kurk, J. D., & Röttgering, H. J. A. 2002, *A&A*, 395, L13
Nakamura, F., McKee, C. F., Klein, R. I., & Fisher, R. T. 2006, *ApJS*, 164, 477
Obergaulinger, M., Iyudin, A. F., Müller, E., & Smoot, G. F. 2014, *MNRAS*, 437, 976
Orlando, S., Bocchino, F., Reale, F., Peres, G., & Pagano, P. 2008, *ApJ*, 678, 274
Orlando, S., Peres, G., Reale, F., Bocchino, F., Rosner, R., Plewa, T., & Siegel, A. 2005, *A&A*, 444, 505
Patnaude, D. J., & Fesen, R. A. 2005, *ApJ*, 633, 240
Pittard, J. M., Dyson, J. E., Falle, S. A. E. G., & Hartquist, T. W. 2005, *MNRAS*, 361, 1077
Pittard, J. M., Falle, S. A. E. G., Hartquist, T. W., & Dyson, J. E. 2009, *MNRAS*, 394, 1351, p09
Pittard, J. M., Hartquist, T. W., & Falle, S. A. E. G. 2010, *MNRAS*, 405, 821
Poludnenko, A. Y., Frank, A., & Blackman, E. G. 2002, *ApJ*, 576, 832
Sales, L. V., Navarro, J. F., Schaye, J., Dalla Vecchia, C., Springel, V., & Booth, C. M. 2010, *MNRAS*, 409, 1541
Shelton, R. L., Kwak, K., & Henley, D. B. 2012, *ApJ*, 751, 120
Shen, F., Feng, X., & Wu, S. T. 2012, in Astronomical Society of the Pacific Conference Series, Vol. 459, Numerical Modeling of Space Plasma Slows (ASTRONUM 2011), ed. N. V. Pogorelov, J. A. Font, E. Audit, & G. P. Zank, 247
Shin, M., Stone, J. M., & Snyder, G. F. 2008, *ApJ*, 680, 336
Stone, J. M., & Norman, M. L. 1992, *ApJL*, 390, L17
van Loo, S., Falle, S. A. E. G., & Hartquist, T. W. 2010, *MNRAS*, 406, 1260
van Loo, S., Falle, S. A. E. G., Hartquist, T. W., & Moore, T. J. T. 2007, *A&A*, 471, 213
Williams, R. J. R., & Dyson, J. E. 2002, *MNRAS*, 333, 1
Yirak, K., Frank, A., & Cunningham, A. J. 2010, *ApJ*, 722, 412

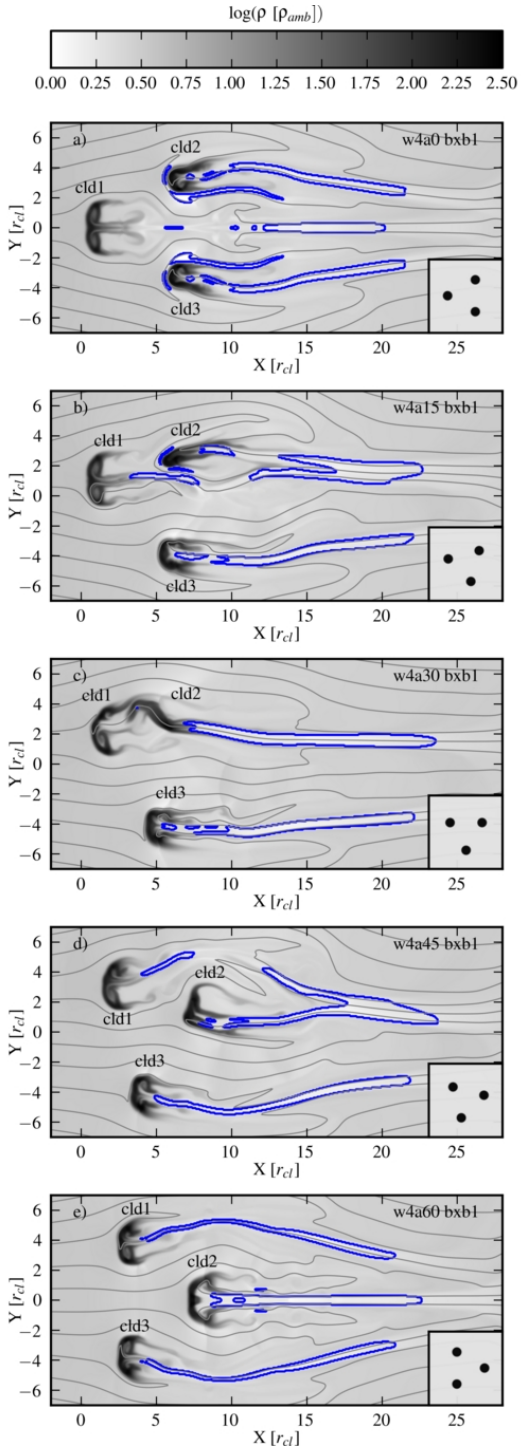

Figure 19. Snapshots at $t = 4\,t_{\rm cc}$ of various 3-cloud simulations with parallel magnetic fields ($\beta_0 = 1.13$). Individual clouds are labelled and the insert shows the initial cloud arrangement in each case. Only the orientation of the cloud arrangement is changed in these cases.

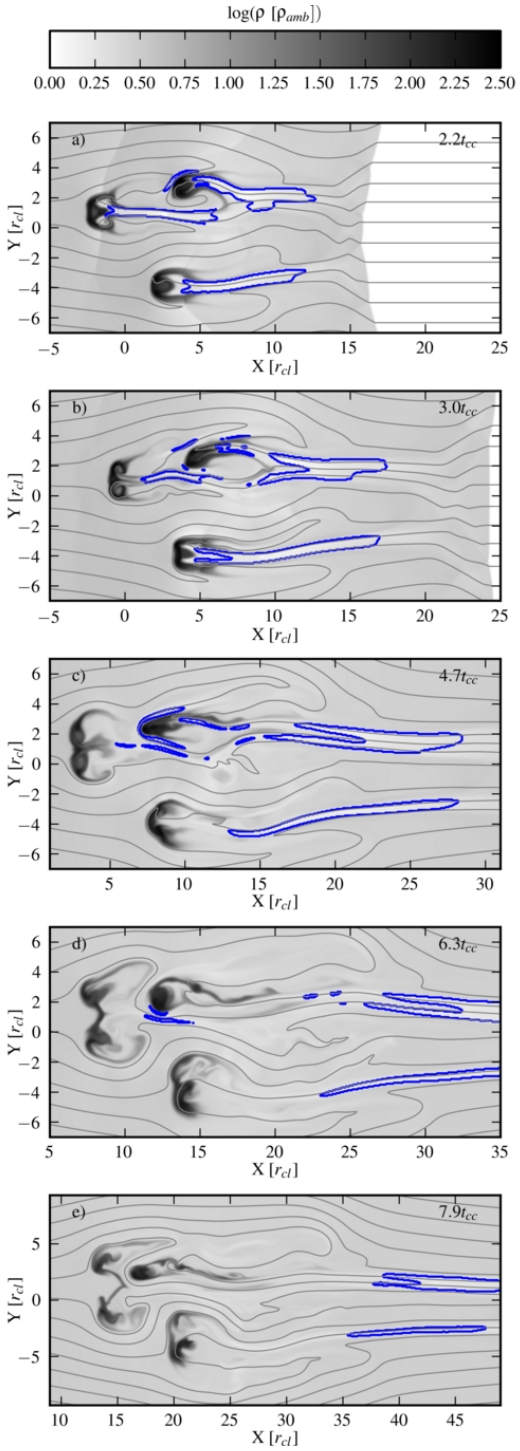

Figure 20. The time evolution of the 3-cloud simulation *s3w4a15* with a parallel magnetic field ($\beta_0 = 1.13$). The logarithmic density and magnetic field evolution are shown at times $t = 2.2$, 3.0, 4.7, 6.3 and 7.9 t_{cc} (top to bottom). The contour shows the "flux-rope" ($\beta < 1$ and $\rho|\mathbf{u}| < 0.5 \times \rho|\mathbf{u}|_{ps}$).

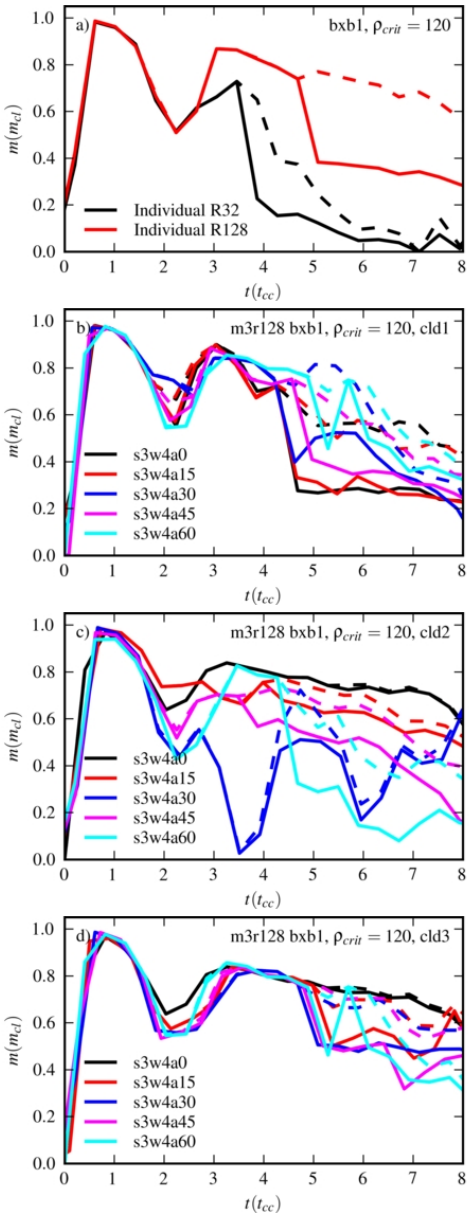

Figure 21. Evolution of the core mass (see text) for a) single cloud simulations at two different resolutions, and for b) cld1, c) cld2 and d) cld3 in high resolution 3-cloud simulations. In each case the solid line represents the main fragment and the dashed line shows the sum of all fragments. The $t = 0$ time for each cloud starts when the shock first reaches the cloud.

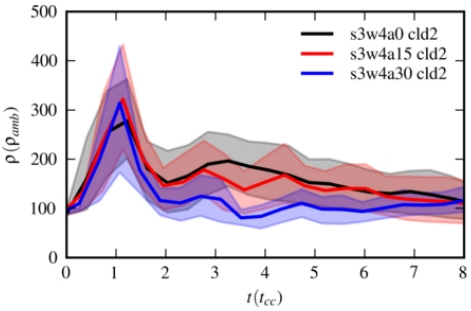

Figure 22. Evolution of the density in cld2 in some of the 3-cloud simulations. The average density within cld2 is shown by the solid line and the region between the 25^{th} and 75^{th} percentiles is shaded.

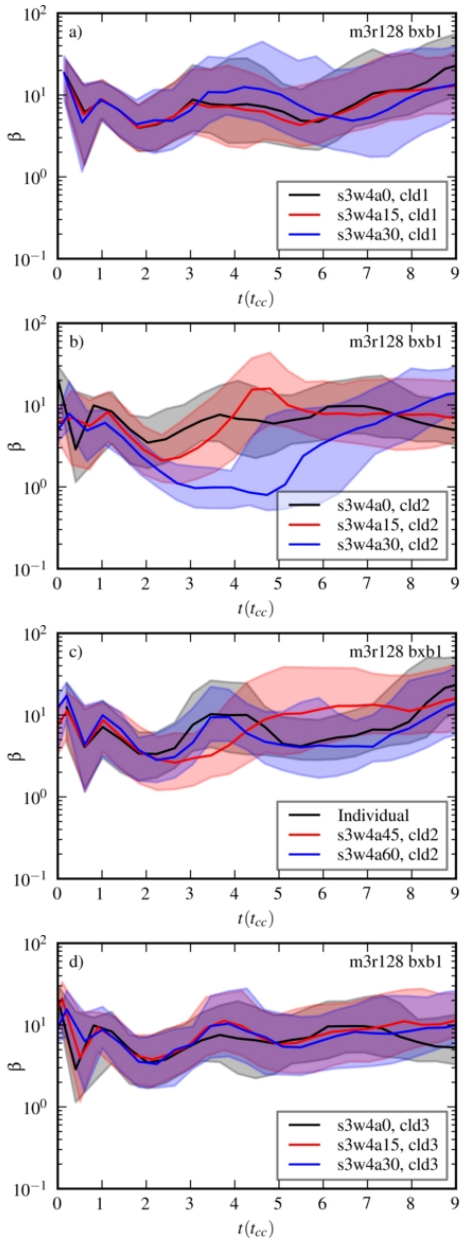

Figure 23. The time evolution of the β distributions for different clouds in high resolution (R_{128}) 3-cloud simulations with parallel magnetic fields and a preshock $\beta = 1.13$. The solid line shows the median value and the area between the 25^{th} and 75^{th} percentiles is shaded.

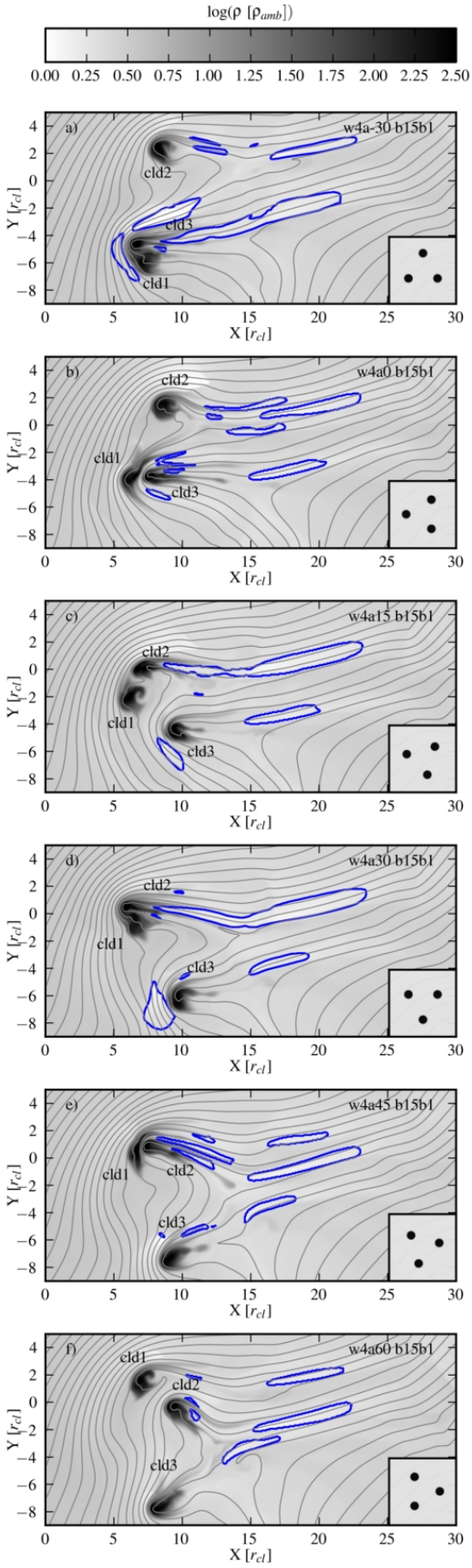

Figure 24. As Fig. 19 but for an oblique shock ($\theta_0 = 15°$, $\beta_0 = 1.13$). All snapshots are at $t = 4\,t_{\rm cc}$.

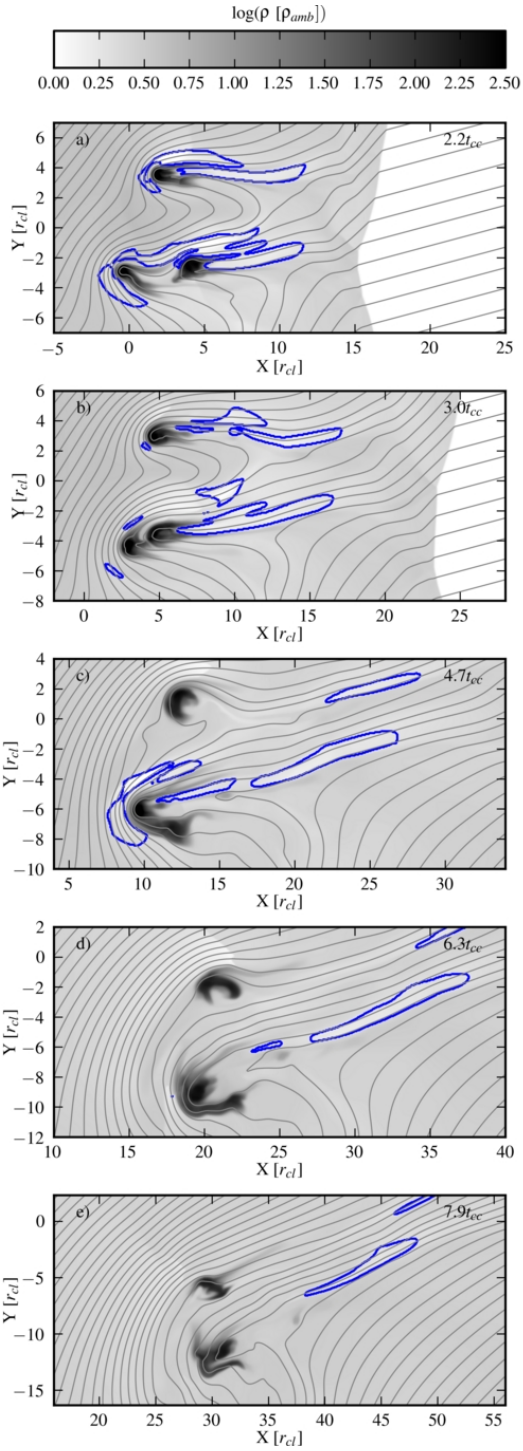

Figure 25. The time evolution of an oblique shock ($\theta_0 = 15°$, $\beta_0 = 1.13$) interacting with 3-clouds (simulation *s3w4a-30*, $a = -30°$).

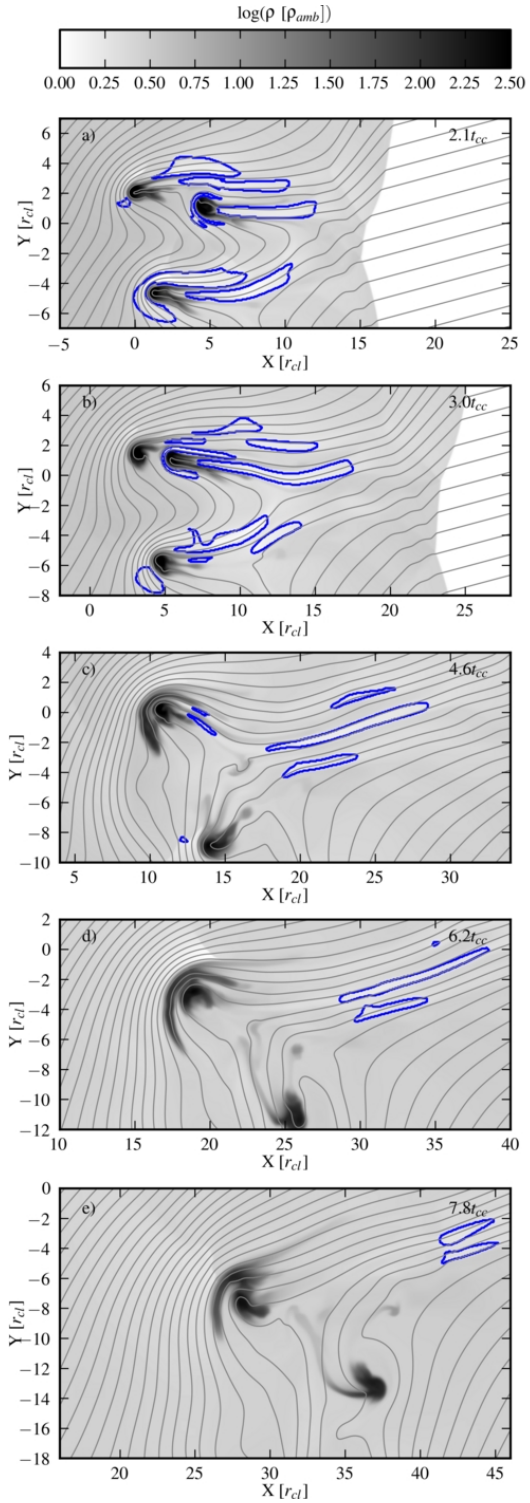

Figure 26. As Fig. 25 but for simulation *s3w4a45* ($\theta_0 = 15°$, $\beta_0 = 1.13$, $a = 45°$).

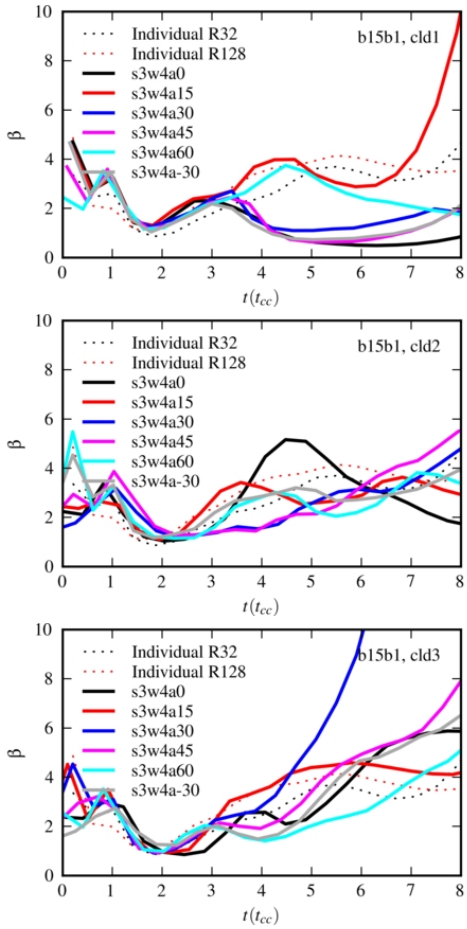

Figure 27. The evolution of the harmonic mean of β for 3-cloud simulations with an oblique magnetic field. The top, middle, and bottom panels show β for cld1, cld2 and cld3 respectively. The time axis is shifted appropriately for each cloud. The evolution of β in isolated clouds is also shown (for simulations with 32 (R_{32}) and 128 (R_{128}) cells per cloud radius).

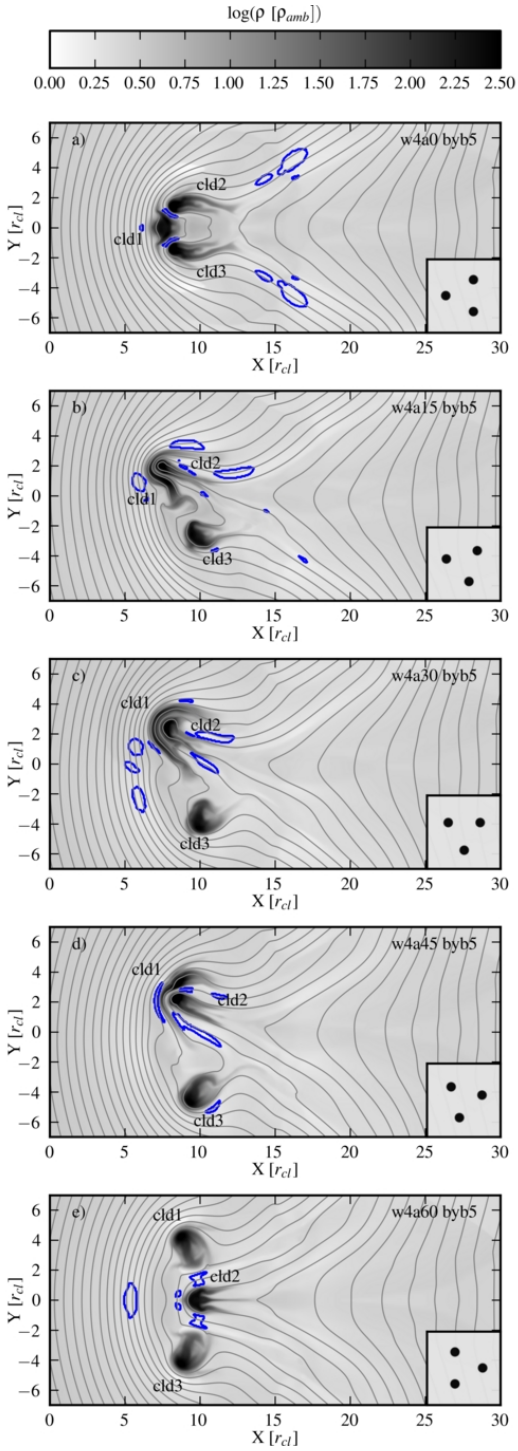

Figure 28. As Fig. 19 but for a perpendicular shock ($\beta_0 = 5.06$). All snapshots are at $t = 4\,t$cc.

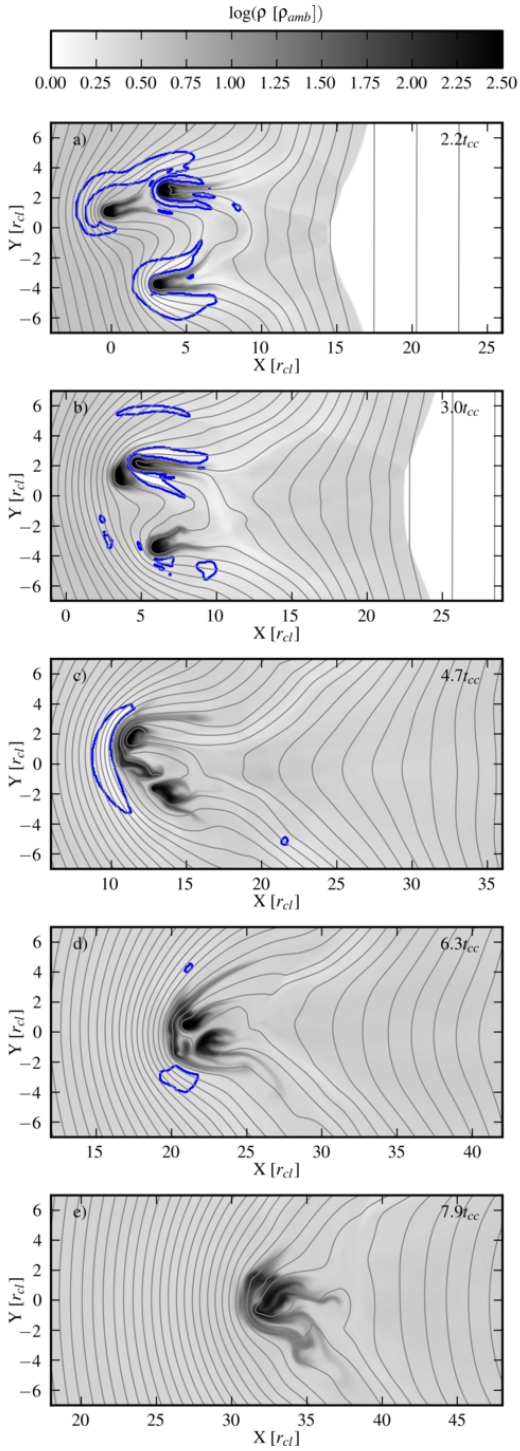

Figure 29. The time evolution of a perpendicular shock interacting with 3 clouds with $\beta_0 = 5.06$ (simulation *s3w4a15*).

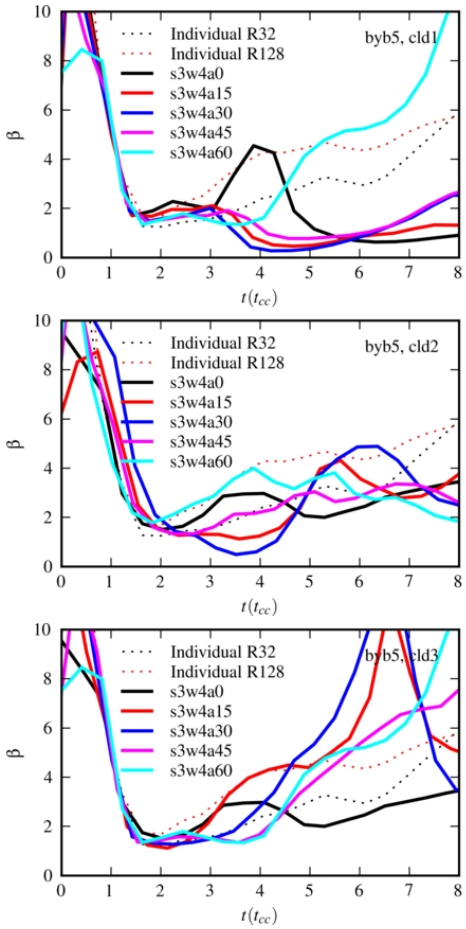

Figure 30. The evolution of the harmonic mean of β for 3-cloud simulations with a perpendicular magnetic field. The top, middle, and bottom panels show β for cld1, cld2 and cld3 respectively. The time axis is shifted appropriately for each cloud. The evolution of β in isolated clouds is also shown (for simulations with 32 (R_{32}) and 128 (R_{128}) cells per cloud radius).